

The magnetic tides of Honolulu

Jeffrey J. Love and E. Joshua Rigler

USGS Geomagnetism Program, Denver, CO 80225, USA. E-mail: jlove@usgs.gov

Accepted 2014 March 10. Received 2014 March 7; in original form 2013 June 28

SUMMARY

We review and analyse the phenomenon of time-invariant, periodic geomagnetic tides. These are generated by the deterministic physics of the ionospheric and oceanic dynamos, and, to a lesser extent, by the solar-quiet magnetosphere, and they are affected by currents induced in the Earth's electrically conducting interior. Using a long historical time-series of hourly magnetic vector measurements made at the Honolulu observatory, we construct high-resolution, frequency-domain power spectra across periods from 0.1 to 10 000.0 d using maximum-entropy and Lomb periodogram algorithms. Recognizing that harmonics corresponding to fundamental forcing periods can, themselves, have amplitude and phase modulation driven by other forcing harmonics, we identify solar-diurnal tides and their annual and solar-cycle sideband modulations, lunar semidiurnal tides and their solar-diurnal sidebands, and tides due to precession of lunar eccentricity and nodes. In contrast to reports by other investigators, we cannot identify tidal signals that might be related to the 22-yr Hale cycle, the Chandler wobble and the quasi-biennial oscillation. Using a least-squares algorithm to estimate the amplitudes and phases of individual tidal constituents, we construct synthetic model time-series that are representative of geomagnetic tidal variation. The signals summarized in this report can be used to test fundamental understanding of the dynamics of the solar-quiet ionosphere and magnetosphere, the ocean and the electrically conducting interior of the Earth, and they can be used to specify a quiet-time baseline against which magnetospheric storm disturbance can be measured.

Key words: Fourier analysis; Tides and planetary waves; Rapid time variations.

1 INTRODUCTION

Tides are periodic oscillations of the Earth sustained by external celestial forces. Most familiar, of course, are oceanic tides. Harmonic ebb and flow in sea level, easily measured with a shore-side tide gauge, is the driven result of gravitational forces that change with the relative motion of the Earth, Moon and Sun (e.g. Hendershott & Munk 1970; Pugh 1987). Gravity also drives atmospheric tides that can be measured, for example, in terms of surface barometric pressure. Even larger atmospheric tides are driven by day-side solar heating and night-side cooling (e.g. Lindzen & Chapman 1969; Volland 1988). The analysis of oceanic and atmospheric tides has a long history (e.g. Cartwright 1999), and the practical need to predict their periods, phases and variational amplitudes added motivation to the 19th century development of classical Fourier time-series methods.

Long ago, the English clockmaker, Graham (1724), discovered the existence of a daily periodic magnetic variation from careful observations of the tiny motion of a compass needle. Subsequently, the amplitude of geomagnetic solar-diurnal variation was found to be modulated over the course of each year, with the orbit of the Earth around the Sun (Canton 1759–1760), and over the

course of each solar cycle, with the waxing and waning of sunspot number (Sabine 1857). Kreil (1852) discovered that compass directional variation measured at the Prague magnetic observatory was correlated with the rotation of the Earth underneath the Moon, and, subsequently, the amplitude of this variation was shown to have a solar-diurnal modulation (Broun 1874, p. 124). Fourier time-series descriptions of periodic geomagnetic variations and their interacting modulations (e.g. Moos 1910; Chapman 1914) are, at least formally, identical to those for oceanic and atmospheric tides. Indeed, in describing diurnal geomagnetic variation, the influential 19th century German geographer and proponent of geomagnetic monitoring, Alexander von Humboldt, used terminology reminiscent of oceanic tides, referring to the ‘magnetische Ebben und Fluten’ (‘magnetic ebb and flow’, Hansteen 1819, p. 459). It is curious, therefore, that the term ‘geomagnetic tide’ has only rarely been used in published literature (e.g. Bartels & Johnston 1940; Fejer 1964; Matsushita 1967; Winch 1981; Olsen 1997), even though it is both accurately descriptive and widely encompassing of relevant physical concepts.

Oceanic and atmospheric tides are the primary sources of magnetic tides. This was, perhaps, first appreciated by Stewart (1882), once the director of the Kew magnetic observatory in London. He

speculated that quiet-time magnetic field variation originated from electric current in a conducting layer of the atmosphere and that this is, somehow, related to high-altitude winds that are driven by day–night differential heating. Stewart was envisioning something that we today call the ‘ionospheric dynamo’: periodic motion of the electrically conducting ionosphere relative to the ambient geomagnetic field induces electric currents, and these, in turn, generate periodic magnetic field variation (e.g. Kelley 1989; Richmond 1995; Heelis 2004). The idea that tidal motion of electrically conducting sea water relative to the ambient geomagnetic field can drive natural induction that contributes to observed magnetic tides (e.g. Larsen 1968; Sanford 1971) seems to have originated with van Bemmelen (1912), once the director of the Batavia magnetic observatory in Java. The amplitudes and phases of magnetic tides, be they generated by dynamos in the ocean, ionosphere or above in the magnetosphere, are modified by induction in the electrically conducting lithosphere. And, indeed, ‘magnetic sounding’ analysis of the Earth’s interior is often performed in the Fourier-transformed (periodic) frequency domain (e.g. Parkinson 1983, Chapter 5; Kuvshinov 2012).

In identifying specific magnetic tidal constituents, we follow convention within the oceanic tidal community (Pugh 1987, p. 12–13; Jay & Kukulka 2003; Lakhani 2005), where a distinction is made between tidal time-invariant periodic signals and those that are not time-invariant periodic. Terrestrial storm and wave phenomena are important and interesting, but they are not well-described as signals with unchanging periodic content and they are not, therefore, ‘tides’. Similar idealized distinctions pertain for our analysis: periodic magnetic tidal variation, also sometimes called ‘quiet-time’ or ‘regular’ variation, is different from magnetic activity that is either fundamentally irregular in time, temporarily ‘quasi-periodic’ or simply not clearly identifiable as periodic. Magnetic storms result from the dynamic interaction of the solar wind with the coupled magnetospheric–ionospheric system. Over long periods of time, the occurrence of magnetic storms can be viewed in terms of probability, with their occurrence likelihood being modulated with the ~ 27 -d Carrington rotation of the Sun, with the semi-annual geoeffectiveness with which the Earth’s magnetosphere is coupled to the solar wind, and with the ~ 11 -yr solar cycle (e.g. Chapman & Bartels 1962, Chapters 11.9, 11.16, 12). Sometimes, magnetic storms interact with magnetic tides, causing a transient enhanced variation at tidal frequencies, but like terrestrial storms and surges seen in tide gauge data, magnetic storms are not, themselves, essentially periodic, and we do not, therefore, consider them to be ‘magnetic tides’.

In this context of history and convention, we choose to review and analyse the time-series and power spectra of magnetic vector data collected over many years at the Honolulu, Hawaii observatory. The relative ease with which large quantities of data can now be analysed on computers permits the construction of spectra having unprecedented frequency resolution. By constructing power spectra from the entire duration of the time-series, we effectively isolate individual time-invariant harmonic constituents of magnetic tides. We can identify (1) the fundamental tidal constituents related to the diurnal rotational period of the Earth, the orbital period of the Earth about the Sun and the orbital period of the Moon about the Earth, (2) fine-structure modulations of the diurnal tides related to the obliquity of the Earth’s rotational axis relative to the ecliptic and the tilt of the Moon’s orbital plane relative to the Earth’s rotational axis and (3) hyperfine modulations related to the precession of the lunar perigee, the solar cycle and the precession of the lunar nodes. We discuss these tidal signals in the context of conventional geophysical interpretations and previously published studies.

2 THE OBSERVATORY AND ITS DATA

The Honolulu magnetic observatory is an integral part of a network of observatories supported by the United States Government for pure and applied geomagnetic science (Love & Finn 2011). The original Honolulu observatory installation was built in 1901 on a magnetically flat ancient coral reef on the south side of the island of Oahu, and routine data acquisition operations commenced in 1902 (CGS 1909). Since then, the observatory has been moved twice, once in 1947 and once in 1960, but each location has been within 10 km distance of the original site (CGS 1963). In terms of operations, from 1902 to 1984, automatic photographic analogue variometers were used to measure continuous relative change in the geomagnetic vector; hourly magnetic field data values were estimated by hand-scaled measurement of paper magnetograms. From 1902 to 1914, reported hourly values were spot measurements centred on the local solar-time hour (00:00, 01:00, etc.), with time measured at the observatory site by the position of the Sun, longitude 202°E . Starting in 1915, reported hourly values were 1-hr boxcar averages of magnetic field components for each whole universal-time hour. Averaging reduces noise, but it also reduces the amplitude of the recorded harmonic signals (Love *et al.* 2010). The time stamps of the hourly averages correspond to the bottom of the universal time hour (00:30, 01:30, etc.) for the hour time zone centred on longitude 195°E (e.g. CGS 1918, p. 5). From 1985 to present, 1-min variometer measurements were acquired by digital electronic systems; these were averaged to form digital hourly values similar to the analogue values. As is standard observatory practice, auxiliary calibration measurements (e.g. Jankowski & Sucksdorff 1996) were combined with the variometer data through processing to produce accurate ‘definitive’ data time-series.

We use 97 years, 1915–2011, of hourly average values of definitive magnetic vectors, which we denote as ‘HON’. Until the end of 2003, these were reported in geographic polar coordinates (H horizontal intensity, D declination, Z vertical down component); starting in 2004, they were reported in geographic Cartesian coordinates (X north, Y east, Z vertical). We focus on (H , D , Z) components, and so we convert (X , Y , Z) when necessary. The duration of the time-series corresponds to 850 296 separate hourly vectors. The discrete time-ordered vector sequences can be denoted as H_i , D_i , Z_i for universal time bottom-of-the-hour time stamps t_i . Approximately 2 per cent of the data values are missing (gaps). We performed an additional analysis (not shown) in which we extended the HON time-series back in time by including the spot value data collected prior to 1915; results were not substantially different from those presented here. Since the Honolulu observatory was moved twice, the historical time-series are, actually, three separate time-series parts, one part for each location with step offsets in the time-series caused by differences in localized permanent crustal magnetization between each site. These offsets have been measured, and they are reported in published observatory yearbooks (e.g. CGS 1963, p. 13). We apply compensating offsets to the three parts of the HON time-series to bring them into temporal continuity. We obtained the HON data values used, here, from the Edinburgh centre of the World Data System.

3 QUIET YEAR 2008

In Figs 1–3, we plot HON H , D and Z data time-series for 2008, a year during which solar-terrestrial conditions were unusually quiet (e.g. Russell *et al.* 2010), sunspots numbers were small,

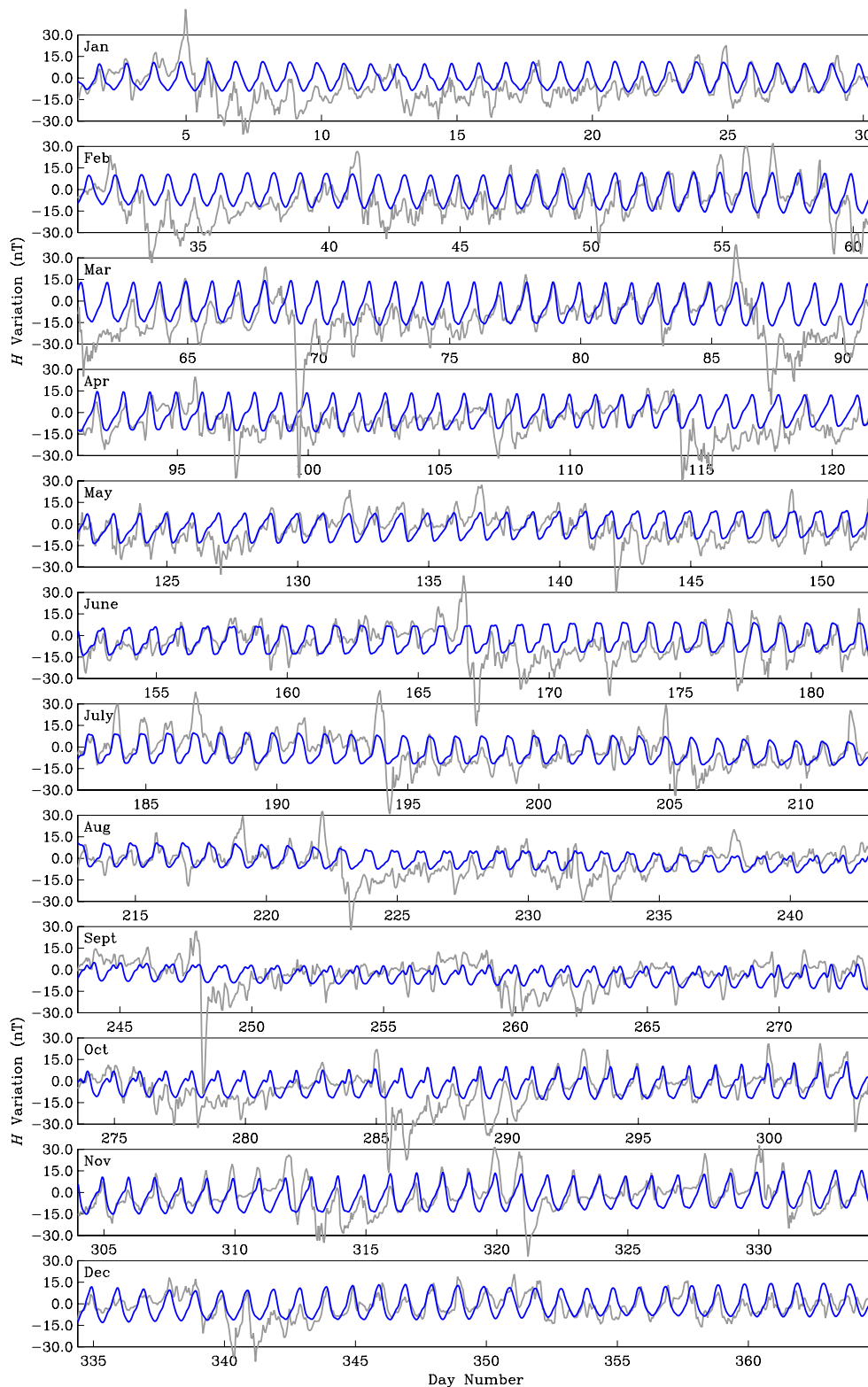


Figure 1. Time-series of HON horizontal intensity H variation for 2008 (grey, Section 2) and a discrete-frequency, synthetic model of long-term average solar-diurnal variation (blue, Section 11). A constant average baseline has been subtracted from each window of time.

coronal mass ejections were infrequent and geomagnetic disturbance was subdued (e.g. Echer *et al.* 2012). Small magnetic storms and irregular activity are seen in H , which records enhancement of the magnetospheric ring current; for example, a storm occurred on September 4 (Day 248). Such non-tidal variation is not nearly so

discernible in either D or Z , and, instead, these vector components mostly just show diurnal variation of slowly changing amplitude and functional character. Clearly seen in D or Z is an annual modulation of the amplitude of the diurnal tide: greatest in the summer, least in the winter.

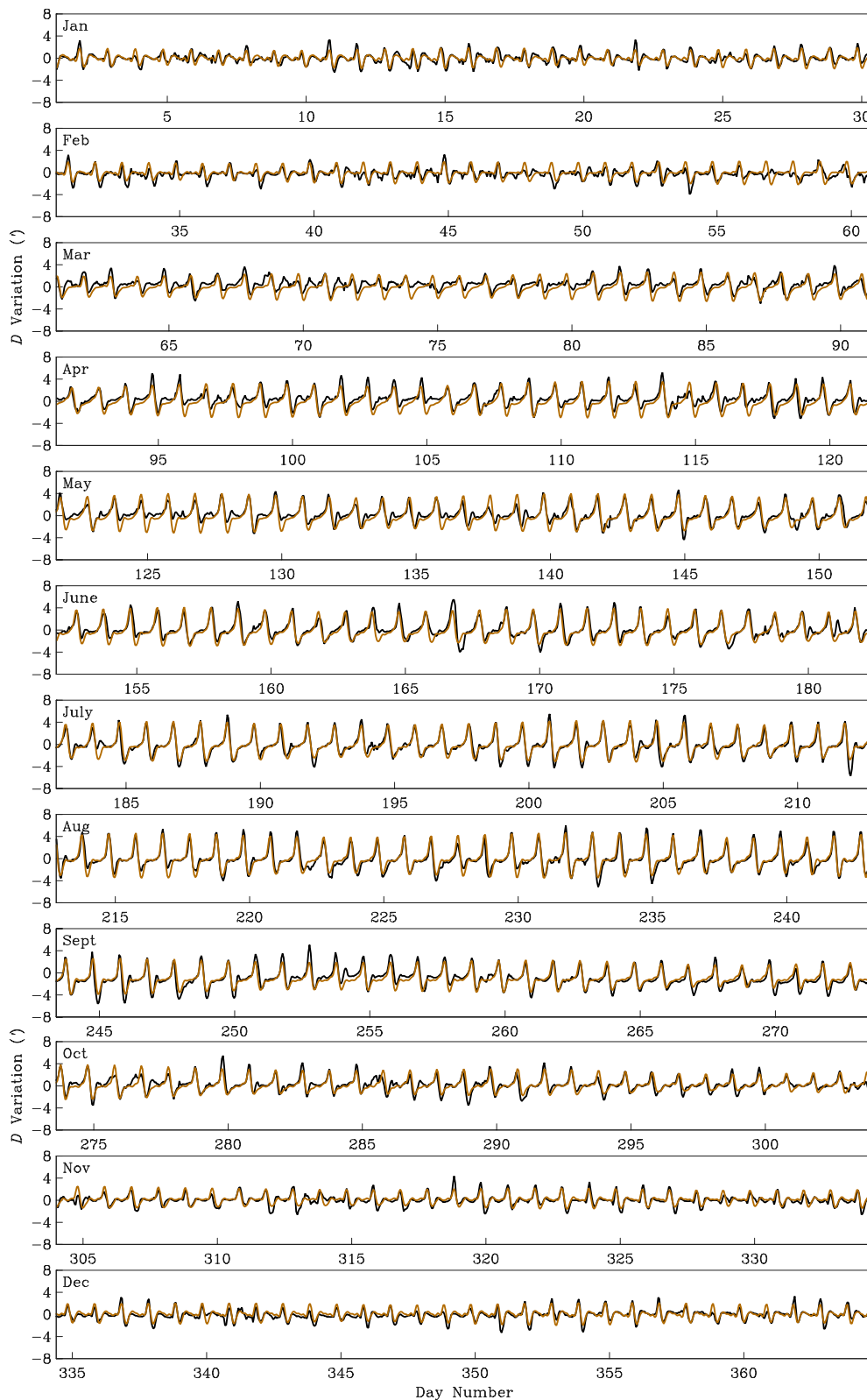


Figure 2. Time-series of HON declination D variation for 2008 (black, Section 2) and a discrete-frequency, synthetic model of long-term average solar-diurnal variation (brown, Section 11). A constant average baseline has been subtracted from each window of time.

4 DIURNAL DYNAMOS

The primary source of diurnal magnetic tidal variation is the thermally driven ionospheric wind dynamo. Day-side solar X-ray and

far-ultraviolet radiation ionizes oxygen atoms, giving electrical conductivity concentrated at ~ 110 km height; electron-ion recombination significantly decreases night-side electrical conductivity. At the same time, day-side solar heating and night-side cooling of the

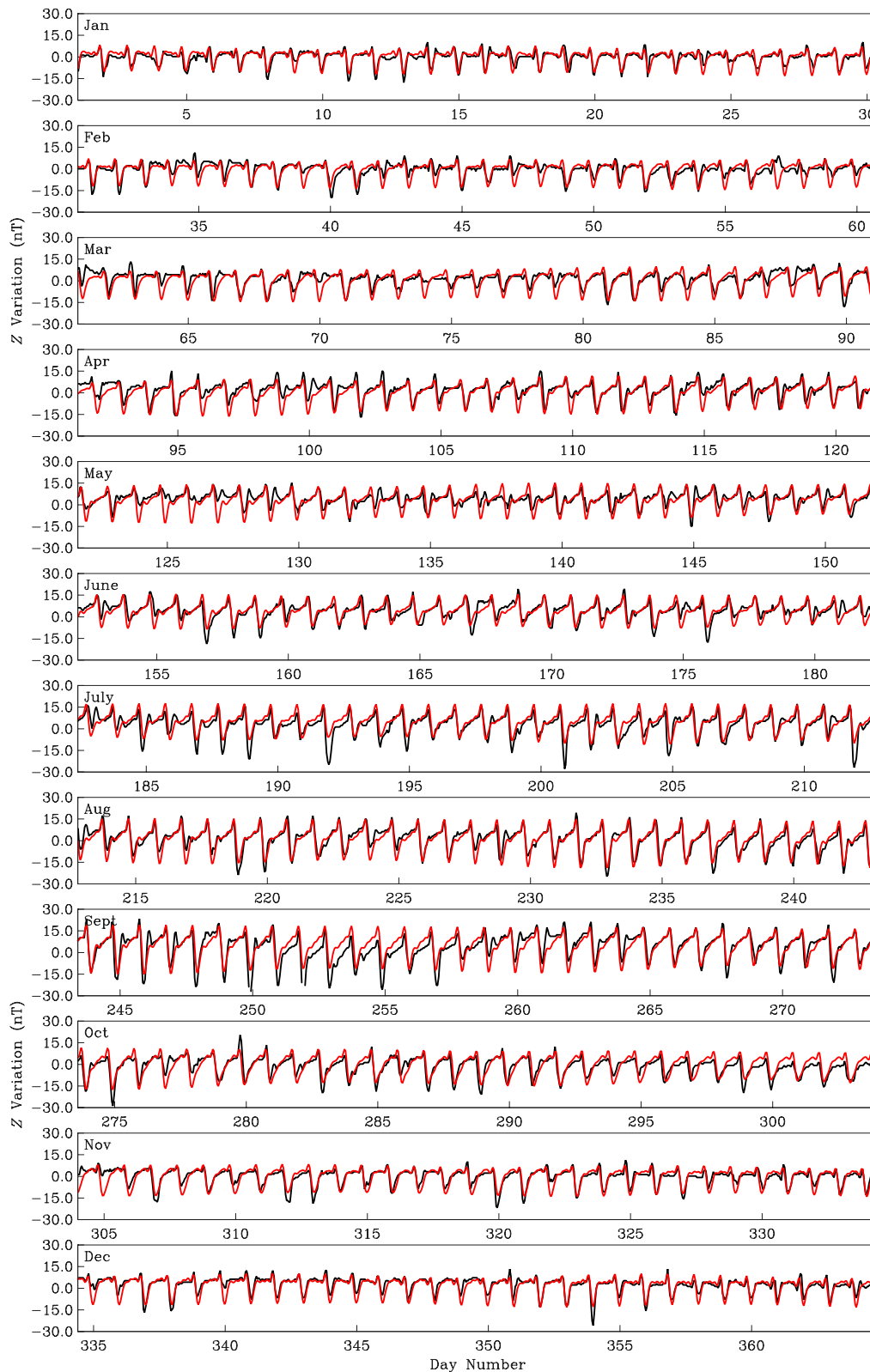


Figure 3. Time-series of HON vertical component Z variation for 2008 (black, Section 2) and a discrete-frequency, synthetic model of long-term average solar-diurnal variation (red, Section 11). A constant average baseline has been subtracted from each window of time.

thermosphere results in a low latitude temperature high at early afternoon local time and a temperature low at early morning. This drives vertical tidal motion and horizontal winds. Concomitant motion of the ionosphere across geomagnetic field lines sustains a day-side,

low latitude, eastward-directed primary electrostatic field (e.g. Stening 1995). This establishes a primary Pedersen current that flows parallel to the electric field. At the dip equator, the main geomagnetic field is horizontal. Ions and electrons, having different radii

of spiral motion around magnetic field lines and different collision frequencies with atmospheric neutrals, drift in opposite directions: ions down and electrons up. The resulting charge separation across the thickness of the equatorial ionosphere produces an upward Hall field, and, with the horizontal magnetic field, this sustains yet another Hall drift: ions east and electrons west. This reinforces the primary Pedersen current, giving the equatorial electrojet (e.g. Kelley 1989, Chapter 3.3). Since ionospheric conductivity is concentrated on the day-side, low latitude eastward currents cannot effectively close through the night-side; they are, instead, forced to close westward at higher day-side latitudes. As a result, the ionospheric current system resembles two large day-side gyres having circulation about foci of opposite polarity that are nearly symmetrically situated on either side, north and south, of the magnetic equator (e.g. Matsushita 1967; Winch 1981).

The gravitationally driven oceanic dynamo is conceptually simpler. Lunar tidal acceleration at a point in the ocean is the local difference between the gravitational attraction of the Moon and the orbital acceleration of the Earth's centre of mass about the barycentre of the Earth–Moon system (e.g. Pugh 1987, Chapter 3). For an idealized solid Earth without continents and covered by an ocean of uniform depth, differential acceleration drives barotropic fluid motion in the ocean, resulting in two equilibrium tidal bulges centred on the Earth–Moon line, one on the Moon-side of the Earth and one on the opposite side of the Earth. If we consider the simple case where the declination of the Moon is nearly zero, that is, when the Moon, in the course of its monthly orbit, is in the equatorial plane of the Earth, then as the Earth rotates underneath the Moon, a semi-diurnal signal, with period corresponding to half a synodic lunar day, is recorded at an oceanic tide gauge. From a frame of reference fixed to the rotating Earth, the two tidal bulges are a poloidal wave in the ocean. Since salt water is electrically conducting, tidal motion of sea water across the main geomagnetic field induces a secondary magnetic field (e.g. Larsen 1968; Sanford 1971). For an idealized geomagnetic field consisting of an axial dipole aligned with the Earth's rotational axis, then, according to fluid mechanical dynamo equations (Bullard & Gellman 1954), a semi-diurnal magnetic tide will be generated; more elaborate, multipolar analyses of oceanic tides have also been accomplished (e.g. Tyler *et al.* 2003). A qualitatively similar process operates in the ionosphere, with gravity affecting an equilibrium tide in the atmosphere, and, therefore, driving barotropic fluid motion of the ionosphere relative to the main geomagnetic field, sustaining yet additional dynamo action.

5 HARMONICS AND MODULATIONS

Under classical tidal analysis, a signal $\zeta(t)$, measured over time at a specified geographic location, is represented as a superposition of discrete Fourier harmonic 'constituents',

$$\zeta(t) = \sum_{\mathbf{k}} \alpha(\mathbf{k}) \cos[\omega(\mathbf{k})t + \phi(\mathbf{k})], \quad (1)$$

where the $\alpha(\mathbf{k})$ are amplitudes, the $\phi(\mathbf{k})$ are phases. A particular angular frequency $\omega(\mathbf{k})$ is a function of the vector \mathbf{k} defined by fundamental periods $T = f^{-1}$ and a vector \mathbf{k} composed of wavenumbers that are an extension of those used by Doodson (1928),

$$\omega(\mathbf{k})/2\pi = \mathbf{k} \cdot \mathbf{f} = k_{\odot}f_{\odot} + k_m f_m + k_a f_a + \dots \quad (2)$$

(e.g. Hendershott & Munk 1970, p. 207). A list of the fundamental periods (and frequencies) considered here is given in Table 1, and a list of specific tidal constituents is given in Table 2. When measuring

Table 1. Some periods and frequencies; $1/T = f = \omega/2\pi$.

	Period		Frequency	
T_{\odot}	1.0000 d	f_{\odot}	1.0000/d	Synodic solar day
	0.9973 d		1.0027/d	Sidereal day
T_{ζ}	1.0351 d	f_{ζ}	0.9661/d	Synodic lunar day
T_m	27.3216 d	f_m	0.0366/d	Sidereal month
	29.5306 d		0.0339/d	Synodic month
T_a	365.2422 d	f_a	1.0000/yr	Tropical year
T_p	8.8475 yr	f_p	0.1130/yr	Sidereal precession of lunar perigee
T_R	~10.4400 yr	f_R	~0.0942/yr	Sunspot solar cycle
T_n	18.6132 yr	f_n	0.0537/yr	Precession of lunar nodes

time relative to the Sun, we use the integers $(k_{\odot}, k_m, k_a)_{\odot}$ for the synodic solar day, $T_{\odot} = 1$ d, sidereal month, $T_m = 27.32$ d and tropical solar year $T_a = 365.24$ d. It is also often convenient to measure time relative to the Moon, using the integers $(k_{\zeta}, k_m, k_a)_{\zeta}$ for the synodic lunar day, $f_{\zeta} = f_{\odot} - f_m + f_a$, where $T_{\zeta} = 1.04$ solar days.

A more elaborate description of magnetic tides can include the secular wave numbers (k_p, k_R, k_n) . Relative sunspot numbers, denoted R , wax and wane over the course of an ~11-yr solar cycle. Concomitant variation in solar insolation drives variation in ionospheric ionization, and, therefore, amplitude modulation of magnetic tides; from HON data, we estimate T_R to be 10.44 yr. Lunar orbital precession also drives tides in the ocean and atmosphere, and, therefore, in the geomagnetic field. Lunar orbital precession is mostly the result of the Sun's gravitational force acting as a torque on the orbital angular momentum vector of the Moon (e.g. Vallado 2007, Chapter 3.7). The component of torque parallel to the angular momentum of the lunar orbit drives precession of ellipticity: the apsidal line that joins the perigee and apogee slowly rotates to the east with period $T_p = 8.85$ yr, thus driving gravitational tides with related frequencies. We follow oceanic tidal convention and refer to these tides as due to 'precession of the lunar perigee'. The component of torque perpendicular to the angular momentum of the lunar orbit drives nodal precession: the lunar orbital plane is inclined relative to the Earth's rotational axis; the intersection of the plane of the moon's orbit with the plane of the Earth's equator defines a line connecting the ascending and descending nodes. As these nodes slowly rotate to the west with period $T_n = 18.61$ yr, the amplitude of lunar declination, the height of the moon in the sky relative to the projection of the Earth's equatorial plane, varies from 18° to 29° , giving a modulation of gravitational tides with related frequencies. We follow oceanic tidal convention and refer to these tides as due to 'precession of the lunar nodes'.

Traditionally, the labels used to identify oceanic tides are those listed by Darwin (1889). In the frequency domain, a multitude of spectral constituents can be identified in oceanic tidal data, for which there are a corresponding multitude of Darwin-labelled letters and numbers (e.g. Cartwright 1999, pp. 100–103). When labelling specific spectral tidal lines (having specific frequencies), we use Darwin symbols. So, for example, the solar-diurnal tide, with frequency f_{\odot} , is denoted S_1 , the solar-semi-diurnal tide, with frequency $2f_{\odot}$, is S_2 , with 'S' for Sun, etc. This labelling should not be confused with the monthly average of solar-quiet daily variation, denoted S_q , and which, itself, changes over the course of a year and solar cycle (e.g. Chapman & Bartels 1962, Chapter 7.8). The basic lunar tide, frequency $2f_{\zeta}$, is denoted M_2 , with 'M' for Moon, etc. And, here, we note that in the geomagnetic community, the letter L is often used to label tides dominated by lunar forcing but which otherwise have a range of frequencies (Chapman & Bartels 1962, Chapter 8).

Table 2. Summary of the Fourier tidal constituents discussed or shown in the figures of this report.

Symbol	Solar k			Lunar k			Secular k			Period	Freq. (c/s.d.)	H		D		Z	
	\odot	m	a	ζ	m	a	p	R	n			A (nT)	ρ (%)	A (°)	ρ (%)	A (nT)	ρ (%)
R	0	0	0	0	0	0	0	1	0	~10.4400 yr	0.0003	8.7858	0.000002	0.4524	0.000005	7.7376	0.000006
S _a	0	0	1	0	0	1	0	0	0	365.2422 d	0.0027	2.8757	0.000004	0.1330	0.000005	2.8131	0.000015
S _{sa}	0	0	2	0	0	2	0	0	0	182.6211 d	0.0055	4.9460	0.000058	0.0632	0.000005	1.7466	0.000016
M _m	0	1	0	0	1	0	-1	0	0	27.5545 d	0.0363	0.5329	0.000027	0.0118	0.000005	0.0659	0.000004
M _{sf}	0	2	-2	0	2	-2	0	0	0	14.7653 d	0.0677	0.6115	0.000135	0.0193	0.000012	0.3545	0.000127
M _f	0	2	0	0	2	0	0	0	0	13.6608 d	0.0732	0.3470	0.000051	0.0076	0.000006	0.0838	0.000011
	0	2	0	0	2	0	0	0	1	13.6334 d	0.0733	0.5296	0.000125	0.0085	0.000006	0.0944	0.000018
Q ₁	1	-3	1	1	1	-2	1	0	0	26.8683 hr	0.8932	0.0494	0.000160	0.0101	0.000330	0.0663	0.000692
	1	-2	0	1	-1	-1	0	0	0	25.8956 hr	0.9268	0.2378	0.003817	0.0165	0.000942	0.1251	0.002491
n	1	-2	1	1	-1	0	0	0	-1	25.8234 hr	0.9294	0.0435	0.000124	0.0046	0.000080	0.1075	0.001912
O ₁	1	-2	1	1	-1	0	0	0	0	25.8193 hr	0.9295	0.3698	0.009265	0.0225	0.001786	0.3380	0.018188
	1	-2	2	1	-1	1	0	0	0	25.7435 hr	0.9323	0.1272	0.001112	0.0363	0.004628	0.3205	0.016422
	1	-2	3	1	-1	2	0	0	0	25.6681 hr	0.9350	0.3576	0.008785	0.0339	0.004071	0.1234	0.002516
	1	-2	4	1	-1	3	0	0	0	25.5932 hr	0.9377	0.3408	0.008020	0.0102	0.000371	0.0546	0.000463
	1	0	-3	1	1	-4	0	0	0	24.1988 hr	0.9918	0.9975	0.076520	0.0418	0.006943	0.0965	0.001775
Π ₁	1	0	-2	1	1	-3	0	0	0	24.1321 hr	0.9945	0.2882	0.006503	0.1114	0.049687	0.7643	0.107679
	1	0	-1	1	1	-2	0	-1	0	24.0722 hr	0.9970	0.4780	0.017852	0.0345	0.004766	0.2669	0.013003
P ₁	1	0	-1	1	1	-2	0	0	0	24.0659 hr	0.9973	1.3147	0.135034	0.3880	0.605148	0.4502	0.037178
	1	0	0	1	1	-1	0	-1	0	24.0063 hr	0.9997	1.4138	0.156791	0.1988	0.159519	1.3513	0.338369
S ₁	1	0	0	1	1	-1	0	0	0	24.0000 hr	1.0000	10.7791	9.109224	1.1886	5.707579	7.0475	9.225083
	1	0	0	1	1	-1	0	1	0	23.9937 hr	1.0003	2.2887	0.410641	0.2034	0.167170	1.3721	0.349760
K ₁	1	0	1	1	1	0	0	0	0	23.9345 hr	1.0027	1.1606	0.106048	0.4003	0.651373	0.6727	0.084960
Φ ₁	1	0	2	1	1	1	0	0	0	23.8693 hr	1.0055	0.3107	0.007689	0.0824	0.027810	0.6315	0.074833
	1	0	3	1	1	2	0	0	0	23.8045 hr	1.0082	0.7187	0.041089	0.0346	0.004942	0.3164	0.019140
J ₁	1	1	1	1	2	0	-1	0	0	23.8766 hr	1.0051	0.2071	0.003667	0.0019	0.000021	0.0266	0.000153
	1	2	-2	1	3	-3	0	0	0	22.4777 hr	1.0677	0.3130	0.008735	0.0252	0.002934	0.1731	0.006449
OO ₁	1	2	1	1	3	0	0	0	0	22.3060 hr	1.0759	0.1697	0.002598	0.0021	0.000025	0.0309	0.000214
N ₂	2	-3	2	2	-1	0	1	0	0	12.6583 hr	1.8960	0.1140	0.003645	0.0305	0.013320	0.1090	0.007755
p	2	-3	3	2	-1	1	1	0	0	12.6401 hr	1.8987	0.0194	0.000111	0.0320	0.014641	0.1111	0.008009
	2	-2	0	2	0	-2	0	0	0	12.4559 hr	1.9268	0.0895	0.002298	0.0427	0.026902	0.1869	0.023839
	2	-2	1	2	0	-1	0	0	0	12.4382 hr	1.9295	0.1380	0.005489	0.0407	0.024535	0.0946	0.006224
M ₂	2	-2	2	2	0	0	0	0	0	12.4206 hr	1.9323	0.5451	0.085593	0.1630	0.394605	0.2535	0.043748
	2	-2	3	2	0	1	0	0	0	12.4030 hr	1.9350	0.1896	0.010386	0.0855	0.108898	0.2721	0.051045
	2	-2	4	2	0	2	0	0	0	12.3855 hr	1.9377	0.1759	0.008986	0.0188	0.005287	0.0948	0.006125
	2	0	-3	2	2	-5	0	0	0	12.0495 hr	1.9918	0.5468	0.091176	0.0641	0.064878	0.3024	0.066683
	2	0	-2	2	2	-4	0	0	0	12.0329 hr	1.9945	0.7574	0.175860	0.0088	0.001211	0.1586	0.018302
	2	0	-1	2	2	-3	0	-1	0	12.0180 hr	1.9970	0.1547	0.007374	0.0364	0.002911	0.1531	0.016851
T ₂	2	0	-1	2	2	-3	0	0	0	12.0165 hr	1.9973	0.7982	0.196075	0.3108	1.529717	1.3534	1.332461
	2	0	-1	2	2	-3	0	1	0	12.0149 hr	1.9975	0.1212	0.004549	0.0462	0.033762	0.1901	0.026099
	2	0	0	2	2	-2	0	-1	0	12.0015 hr	1.9998	0.7052	0.153444	0.1361	0.294118	0.7078	0.365481
S ₂	2	0	0	2	2	-2	0	0	0	12.0000 hr	2.0000	2.6539	2.171330	1.1579	21.297134	4.5346	15.021479
	2	0	0	2	2	-2	0	1	0	11.9985 hr	2.0002	0.6508	0.130492	0.1313	0.273762	0.7056	0.364055
	2	0	1	2	2	-1	0	-1	0	11.9852 hr	2.0025	0.0305	0.000288	0.0596	0.005624	0.1960	0.027932
R ₂	2	0	1	2	2	-1	0	0	0	11.9836 hr	2.0027	0.3936	0.047710	0.3974	2.515496	1.3124	1.259504
K ₂	2	0	2	2	2	0	0	0	0	11.9672 hr	2.0055	1.1433	0.405308	0.0681	0.073914	0.2017	0.029573
	2	0	3	2	2	1	0	0	0	11.9509 hr	2.0082	0.4977	0.076834	0.1272	0.259210	0.5459	0.220254
2SM ₂	2	2	-2	2	4	-4	0	0	0	11.6070 hr	2.0677	0.1386	0.006304	0.0107	0.001948	0.0590	0.002770
p	3	-3	2	3	0	-1	1	0	0	8.2873 hr	2.8960	0.0398	0.001015	0.0203	0.013465	0.0827	0.010253
p	3	-3	3	3	0	0	1	0	0	8.2795 hr	2.8987	0.0230	0.000344	0.0183	0.010875	0.0795	0.009388
	3	-2	0	3	1	-3	0	0	0	8.2001 hr	2.9268	0.0345	0.000774	0.0278	0.025633	0.1234	0.023427
	3	-2	1	3	1	-2	0	0	0	8.1924 hr	2.9295	0.0514	0.001707	0.0170	0.009605	0.0529	0.004374
	3	-2	2	3	1	-1	0	0	0	8.1848 hr	2.9323	0.1498	0.014459	0.0850	0.240010	0.3472	0.183732
MK ₃	3	-2	3	3	1	0	0	0	0	8.1771 hr	2.9350	0.0998	0.006446	0.0561	0.104840	0.2326	0.083350
	3	-2	4	3	1	1	0	0	0	8.1695 hr	2.9377	0.0741	0.003574	0.0129	0.005604	0.0640	0.006362
	3	0	-3	3	3	-5	0	0	0	8.0220 hr	2.9918	0.2127	0.030190	0.0420	0.060934	0.2403	0.092169
	3	0	-2	3	3	-5	0	0	0	8.0146 hr	2.9945	0.5986	0.240265	0.0491	0.083440	0.2497	0.098689
	3	0	-1	3	3	-4	0	0	0	8.0073 hr	2.9973	0.5371	0.194327	0.2744	2.609287	1.2408	2.453068
	3	0	-1	3	3	-4	0	1	0	8.0066 hr	2.9975	0.0872	0.005107	0.0276	0.026277	0.1291	0.026504
	3	0	0	3	3	-3	0	-1	0	8.0007 hr	2.9997	0.3123	0.065836	0.0827	0.237314	0.4162	0.276915
S ₃	3	0	0	3	3	-3	0	0	0	8.0000 hr	3.0000	0.5937	0.237516	0.6115	12.987240	2.8200	12.704157
	3	0	0	3	3	-3	0	1	0	7.9993 hr	3.0003	0.2293	0.035389	0.0774	0.208269	0.4049	0.262683
	3	0	1	3	3	-2	0	-1	0	7.9934 hr	3.0025	0.0381	0.000990	0.0333	0.038603	0.1607	0.040950
	3	0	1	3	3	-2	0	0	0	7.9927 hr	3.0027	0.3890	0.102378	0.3171	3.496562	1.4423	3.324580
	3	0	2	3	3	-1	0	0	0	7.9854 hr	3.0055	0.5959	0.240068	0.0813	0.230410	0.3638	0.211379

Downloaded from <http://journals.oxfordjournals.org/> at USGS Libraries on May 19, 2014

Table 2. (Continued.)

Symbol	Solar k			Lunar k			Secular k			Period	Freq. (c/s.d.)	H		D		Z	
	\odot	m	a	ζ	m	a	p	R	n			A (nT)	ρ (%)	A (°)	ρ (%)	A (nT)	ρ (%)
K_3	3	0	3	3	3	0	0	0	0	7.9782 hr	3.0082	0.3382	0.077260	0.0998	0.348177	0.4650	0.348015
MS_4	4	-2	2	4	2	-2	0	0	0	6.1033 hr	3.9323	0.1207	0.016214	0.0299	0.051154	0.1358	0.048559
MK_4	4	-2	4	4	2	0	0	0	0	6.0949 hr	3.9377	0.0098	0.000111	0.0110	0.006973	0.0500	0.006767
	4	0	-3	4	4	-7	0	0	0	6.0123 hr	3.9918	0.1107	0.013999	0.0025	0.000386	0.0635	0.011110
	4	0	-2	4	4	-6	0	0	0	6.0082 hr	3.9945	0.2643	0.079947	0.0515	0.157025	0.2584	0.181306
	4	0	-1	4	4	-5	0	0	0	6.0041 hr	3.9973	0.1510	0.026322	0.1708	1.727428	0.8091	1.783827
S_4	4	0	0	4	4	-4	0	0	0	6.0000 hr	4.0000	0.5343	0.328243	0.2324	3.203325	1.1081	3.349408
	4	0	1	4	4	-3	0	0	0	5.9959 hr	4.0027	0.2853	0.093893	0.1444	1.236747	0.7513	1.540682
	4	0	2	4	4	-2	0	0	0	5.9918 hr	4.0055	0.1628	0.030475	0.0666	0.263179	0.3067	0.256683
	4	0	3	4	4	-1	0	0	0	5.9877 hr	4.0082	0.1860	0.039811	0.0215	0.027487	0.1341	0.049584
K_4	4	0	4	4	4	0	0	0	0	5.9836 hr	4.0110	0.0995	0.011533	0.0239	0.033984	0.1377	0.052364
	5	0	-2	5	5	-7	0	0	0	4.8053 hr	4.9945	0.0747	0.009554	0.0244	0.052104	0.1427	0.082543
	5	0	-1	5	5	-6	0	0	0	4.8026 hr	4.9973	0.0832	0.011848	0.0963	0.813935	0.5044	1.028453
S_5	5	0	0	5	5	-5	0	0	0	4.8000 hr	5.0000	0.1048	0.018852	0.0571	0.286078	0.3284	0.434832
	5	0	1	5	5	-4	0	0	0	4.7974 hr	5.0027	0.0982	0.016443	0.0723	0.459865	0.3702	0.555653
	5	0	2	5	5	-3	0	0	0	4.7947 hr	5.0055	0.0611	0.006353	0.0060	0.003131	0.0410	0.006906
S_6	6	0	0	6	6	-6	0	0	0	4.0000 hr	6.0000	0.1825	0.076605	0.0297	0.104435	0.1260	0.086163

In the oceanic tidal community, the letter L is used as a label for a specific spectral tidal line (having a specific frequency). We avoid ambiguity by using the more specific oceanic labelling of Darwin.

Much of the intricate structure in magnetic tidal spectra can be understood, qualitatively, in terms of superposition and a combination of amplitude and phase modulation. First, consider, as an idealized example, the superposition of two basic half-day tides: the lunar phase semi-diurnal M_2 tide and the solar S_2 gravitational tide, each of them are familiarly observed in oceanic tides (e.g. Pugh 1987, eq. 4:2),

$$\zeta(t) = \cos [2\omega_{\zeta}t] + \cos [2\omega_{\odot}t], \tag{3}$$

where, for clarity, we have dropped constant phase factors. After applying a simple trigonometric identity,

$$\zeta(t) = 2 \cos [(\omega_{\odot} + \omega_{\zeta})t] \cos [(\omega_{\odot} - \omega_{\zeta})t]. \tag{4}$$

From this, we understand that part of the observed tidal variation can be expressed as a carrier signal with frequency $f_{\odot} + f_{\zeta}$, corresponding to a period of 12.21 hr. Over the course of a synodic month, the sign of the modulation term oscillates from positive to negative, but the beat amplitude is given by the absolute value of the modulation term, and this has a period of half a synodic month, frequency $2f_{\odot} - 2f_{\zeta} = 2f_m - 2f_a$ and period 14.77 d. The largest amplitude—‘spring’—occurs during new and full-Moon syzygy; the smallest amplitude—‘neap’—occurs during lunar first and third quarter-Moon quadrature (e.g. Pugh 1987, Chapter 3:4:2). More generally, amplitude modulation of a carrier harmonic results in a split pair of sideband constituents, with one constituent having a frequency equal to the sum of the carrier and modulation frequencies, and the other equal to their difference.

Next, consider the solar-diurnal tide S_1 . Due to the obliquity of the Earth’s rotational axis relative to the ecliptic, and the eccentricity of the Earth’s orbit around the Sun, the observed position of the Sun in the sky traces out a figure eight analemma in declination and ascension over the course of a year. Concomitant change in insolation and day–night differential heating results in amplitude and phase modulation of ionospheric S_1 . For illustration, we consider only phase modulation and write

$$\zeta(t) = \alpha_{\odot} \cos [\omega_{\odot}t + \phi \sin(\omega_a t)]. \tag{5}$$

After applying the Jacobi–Anger formula (e.g. Korn & Korn 2000, Chapters 21.8-4), eq. (5) can be expressed in terms of discrete Fourier constituents having Bessel function J_{k_a} amplitudes,

$$\zeta(t) = \alpha_{\odot} \sum_{k_a=-\infty}^{k_a=+\infty} J_{k_a}(\phi) \cos [(\omega_{\odot} + k_a \omega_a)t], \tag{6}$$

that are separated in frequency, like a comb, by integer multiples of the modulation frequency and where amplitudes are symmetrically arranged about the carrier frequency.

6 SPECTRUM CONSTRUCTION

A frequency-domain power spectrum constructed from a data time-series using a maximum-entropy method identifies a finite set of deterministic autoregressive time lags as singular ‘poles’ and, otherwise, maximizes the ‘whiteness’ (maximizes the ‘entropy’) of background noise (e.g. Kanasewich 1981, Chapter 11.3). Therefore, a maximum-entropy algorithm is useful for identifying the frequencies of periodic harmonic constituents and for resolving constituents having similar frequencies. A maximum-entropy algorithm is not useful for estimating corresponding constituent power (Press *et al.* 1992, p. 566; Emery & Thomson 2001, p. 465), since it outputs a numerical ‘approximation’ of infinite power density at a finite number of discrete points along the frequency continuum. We construct maximum-entropy spectra for each magnetic vector component using a Burg algorithm (Press *et al.* 1992, Chapters 13.6–13.7, ‘memcof’ and ‘evlmem’); the average level of the output power spectrum is normalized by dividing by the variance of the input data. Maximum-entropy spectrum algorithms are parametric; one must specify M , the order of the autoregressive approximation; the higher (lower) the order the greater (lower) the number of poles in the spectrum. We discuss selection of the maximum-entropy M parameter below.

In contrast, a periodogram power spectrum is constructed assuming that a given data time-series can be well-described in terms of a moving-average noise model having harmonic power across a continuous range of frequencies. A periodogram algorithm provides an estimate of the average spectral power over a discrete set of finite-differentials of frequency, the widths of each differential being limited by the inverse of the product of the number of data and

the sampling interval. For a finite number of data values, sine and cosine amplitudes are often obtained by fast-Fourier transformation, but they can also be obtained, as we implement, by least-squares fitting with a numerically efficient Lomb algorithm (Press *et al.* 1992, Chapter 13.8, ‘faster’). Like the maximum-entropy algorithm, the output Lomb power spectrum is normalized by the variance of the input data. Separately, we also fit individual Fourier constituents to each HON magnetic vector time-series using a least-squares algorithm; we invert for amplitudes and phases for a specified set of constituent frequencies.

Different methods for constructing frequency-domain spectra are based on different theoretical assumptions and will, therefore, give different results (e.g. Ghil & Taricco 1997, Section 7). We are confident in interpreting tidal signals that can be consistently identified in spectra constructed by both maximum likelihood and Lomb periodogram methods (see recommendation in Press *et al.* 1992, p. 567). We choose the maximum-entropy M parameter so that the output spectra generally resembles that from the Lomb algorithm, seeking a maximum-entropy spectrum that is not too spiky and not too smooth and with M set just large enough to resolve tidal constituents that we expect are present in the data. In our analysis, $M = 150\,000$, a factor 5.6 smaller than the number of data in the 97-yr time-series. We prepare the input HON time-series for the maximum-entropy and Lomb periodograms in exactly the same way. We interpolate over data gaps, even though the Lomb algorithm does not require this. We ‘pre-whiten’ by first-differencing (Blackman & Tukey 1958, Chapter 15; Emery & Thomson 2001, p. 457), so $\Delta H_i = H_{i+1} - H_i$, etc. This shifts the distribution of power so that a naturally ‘red’ spectrum, dominated by power at low frequencies, is changed to one that is more ‘blue’, with greater power at higher frequencies. In the case of the HON spectra, power is shifted closer to the diurnal frequencies of most interest in our analysis. All computer programs are compiled with 64-bit float-point precision.

7 BROAD PERSPECTIVE

In Fig. 4(a) we plot maximum-entropy power spectra, and in Fig. 4(b) we plot Lomb power spectra, each for first-differences (Δ) of HON horizontal-intensity H , declination D and vertical component Z data over periods ranging from 10 000.0 to 0.1 d. Both algorithms clearly show numerous spectral lines, but the maximum-entropy spectra show line heights that are more substantially above background noise than do the Lomb periodogram spectra; we emphasize that here, and for all the spectral plots that follow, vertical scales are logarithmic, and so in many cases the identified tidal constituents are easily differentiated from background noise. A list of the numerous tidal spectral constituents identified in this report is given in a Table 2. At the high-frequency end of Fig. 4, all three vector components show groups of diurnal lines, these being associated with the solar tides S_{k_\odot} , with frequencies $k_\odot f_\odot$, where $k_\odot = 1 - 9$. In more detail, in Fig. 4(b) we note that tidal amplitudes for the diurnal H component are closer to the background noise level than for either of D or Z . This difference can be attributed to the equatorial ring current of the magnetosphere, which generates non-tidal activity that is primarily in the geomagnetic north–south H direction, thus lifting the level of background noise for this component.

In the middle of the frequency range of Figs 4(a) and (b), the spectrum for Z shows the synodic fortnightly lunar tide, labelled M_{sf} and having frequency $2f_\odot - 2f_\zeta = 2f_m - 2f_a$. This particular constituent has the same frequency as the neap-spring modulation term discussed in Section 5. According to gravitational potential

theory, the M_{sf} oceanic tide would normally have a relatively small amplitude compared to other lunar-tidal spectral line neighbours (e.g. Cartwright & Tayler 1971, table 4a, Group 0). For example, comparing M_{sf} with the amplitude of the sidereal monthly tide M_m , frequency $f_m - f_p$, we find that $M_m/M_{sf} = 6.04$; comparing M_{sf} with the amplitude of the fortnightly tide M_f , frequency $2f_m$, we find that $M_f/M_{sf} = 11.45$. On the other hand, in coastal shallow water settings, non-linear effects modify potential theory amplitudes, and sometimes M_{sf} is a prominent tide (e.g. Pugh 1987, Chapter 4:2:3). That the M_{sf} tide is also prominent in HON magnetic data, while M_m and M_f are not even discernible above noise, might mean that the role of the gravitationally driven oceanic dynamo is very small. We speculate that magnetic M_{sf} is supported by non-linear ionospheric dynamics.

At the low-frequency ends of the maximum-entropy spectra, Fig. 4(a), H and Z show both annual S_a and semiannual S_{sa} tides; neither are evident in D . These tides (e.g. Campbell 1982) are generally considered to be distinct from the semi-annual modulation of magnetic disturbance (e.g. Chapman & Bartels 1962, Chapter 11.9). Most low latitude magnetic observatories record a semi-annual tide in H , with maximum amplitude at about the time of equinox when the two day-side current gyres are of approximately equal strength, thus reinforcing each other at the equatorial electrojet (Chapman & Raja Rao 1965; Rastogi 1993, p. 569). In Fig. 4(a) there is a hint of the ~ 11 -yr sunspot solar cycle, labelled R. This spectral constituent is prominent in magnetic index time-series that are specifically designed to measure (non-tidal) magnetic disturbance (e.g. Courtillot *et al.* 1977), but also see Section 11. We note that the Lomb periodogram spectra show considerably more noise at low frequencies, and, indeed, they do not clearly show annual or solar-cycle tidal constituents. In Section 9, we identify solar-cycle modulation of solar-diurnal S_{k_\odot} . In terms of other fundamental tidal periods, neither the maximum-entropy nor the Lomb-periodogram show a $T_p = 8.85$ -yr spectral line corresponding to perigee precession, nor do they show a $T_n = 18.61$ -yr line corresponding to nodal precession. As we will discuss in Section 9, these long-period harmonics modulate diurnal tidal constituents. For now, we simply note, from discussion in Section 5, that simple harmonic amplitude modulation, such as described by the multiplication of two Fourier harmonics, will not, in general, give a spectral line at the modulation frequency.

8 FINE STRUCTURE

In Fig. 5, we note the spectral fine structure surrounding the solar-diurnal, semi-diurnal, etc. constituents S_{k_\odot} (e.g. Chapman & Bartels 1962, Chapter 7). Close by the fundamental period S_1 is the spectral line labelled K_1 . With frequency $f_\odot + f_a$, this might be considered to be a sidereal-diurnal tide, defined by Earth’s rotation relative to the stars, not the Sun. Some time ago, before detailed magnetic tidal spectra could be easily constructed, Campbell (1972) speculated that a sidereal tide might be the result of ionospheric ionization from galactic X-rays. Subsequently, Malin (1973) noted that a sidereal magnetic tide could have several causes related to more traditional tidal dynamics. We note, for example, that K_1 is prominent in spectra of oceanic tide gauge data, where lunar-orbital declination results in monthly amplitude modulation of the lunar-diurnal carrier tide. This, then, corresponds to a split pair of tides having approximately equal amplitudes, K_1 and O_1 , with frequencies $f_\zeta \pm f_m$ (e.g. Pugh 1987, table 4:1). The K_1 tide has the degeneracy $f_\zeta + f_m = f_\odot + f_a$, so at least part of the sidereal-diurnal tide could arise from the gravitational dynamo in either the ocean or

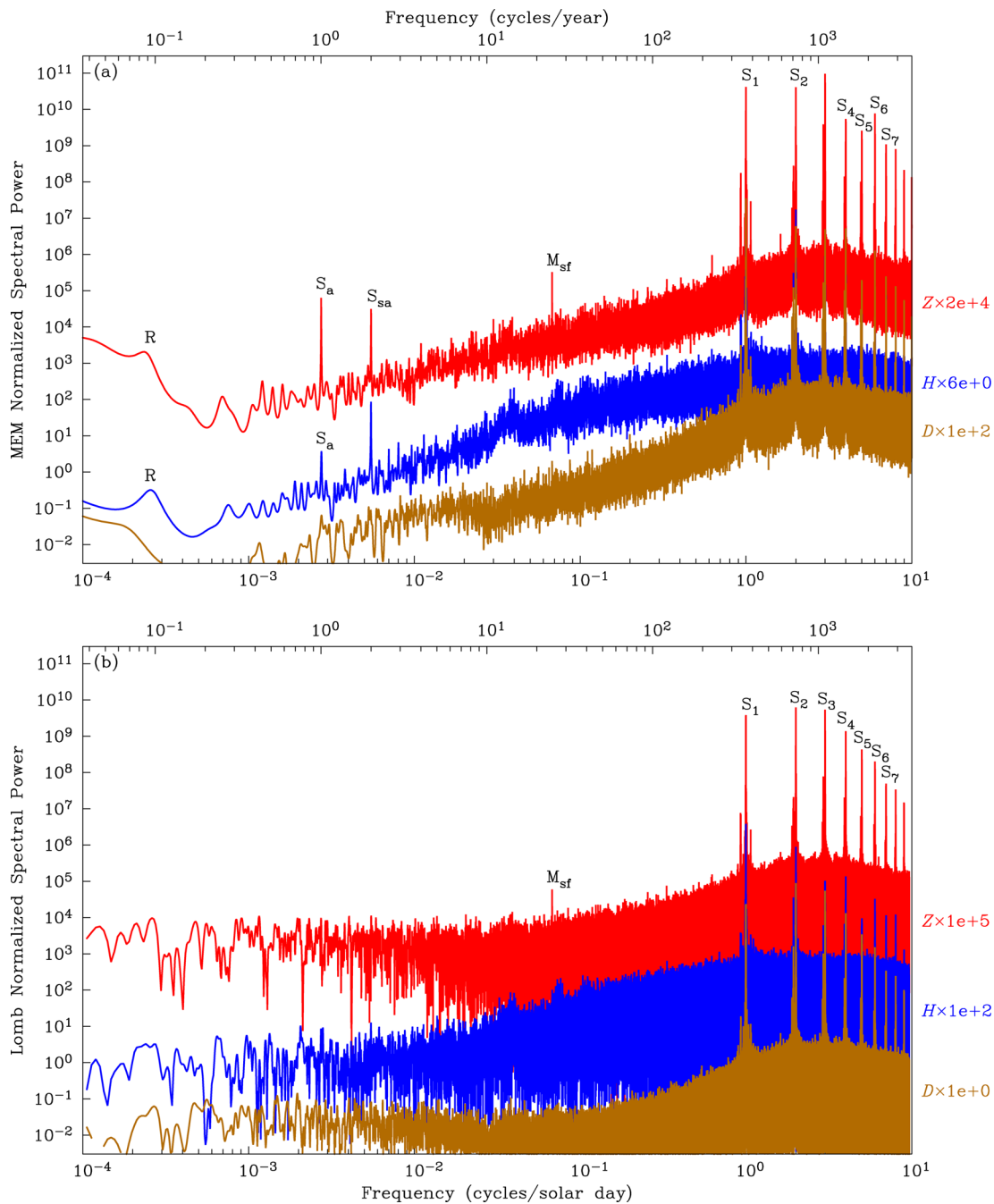


Figure 4. Maximum-entropy spectra (a) and Lomb periodogram spectra (b) of pre-whitened first differences (Δ) of HON H (blue), D (brown), Z (red) as a function of solar day and year frequency. Multiplicative factors, indicated in the right margin, are applied for purposes of clarity.

ionosphere. Upon looking across the vertical extent of Figs 5(a)–(d), we recognize that it is reasonable to regard magnetic K_1 as just one of many sideband constituents in tightly spaced spectral line combs that, as discussed in Section 5, arise from phase modulation, $k_{\odot}f_{\odot} + k_a f_a$ (e.g. De Meyer 1980; Nowożyński 2006).

Next, we note the fine structure surrounding lunar constituents (e.g. Chapman & Bartels 1962, Chapter 8). The spectral line corresponding to the basic lunar semi-diurnal tide M_2 is prominently seen in Fig. 5(b) surrounded by an annual constituent comb of lines, frequencies $2f_{\zeta} + k_a f_a$. Another set of spectral sideband combs is seen across the vertical extent of Figs 5(a)–(d), including the constituents O_1 , M_2 , MK_3 and MS_4 . These combs are separated by frequencies consistent with solar-diurnal and solar-annual modula-

tion of the basic lunar semi-diurnal tide, $2f_{\zeta} + k_{\odot}f_{\odot} + k_a f_a$. Previous projects that focussed on identifying the existence of the O_1 constituent (Winch 1970; Tarpley 1971; Rao & Sastri 1974; Maus & Kuvshinov 2004) were motivated by an interest in assessing the relative contributions of the ionospheric and oceanic dynamos for magnetic tides, but detailed spectra could not be constructed for those projects because of limited computer power. Having now obtained high resolution spectra, we recognize the role of lunar gravitation, but we also recognize that gravity can affect both the ionospheric and oceanic dynamos. Other analyses have used night-side subsampling of observatory data to try to separate signals from the oceanic and ionospheric dynamos (Malin 1970); we have not attempted such an analysis here. In Fig. 5(b) there is a faint line marked $2SM_2$ that

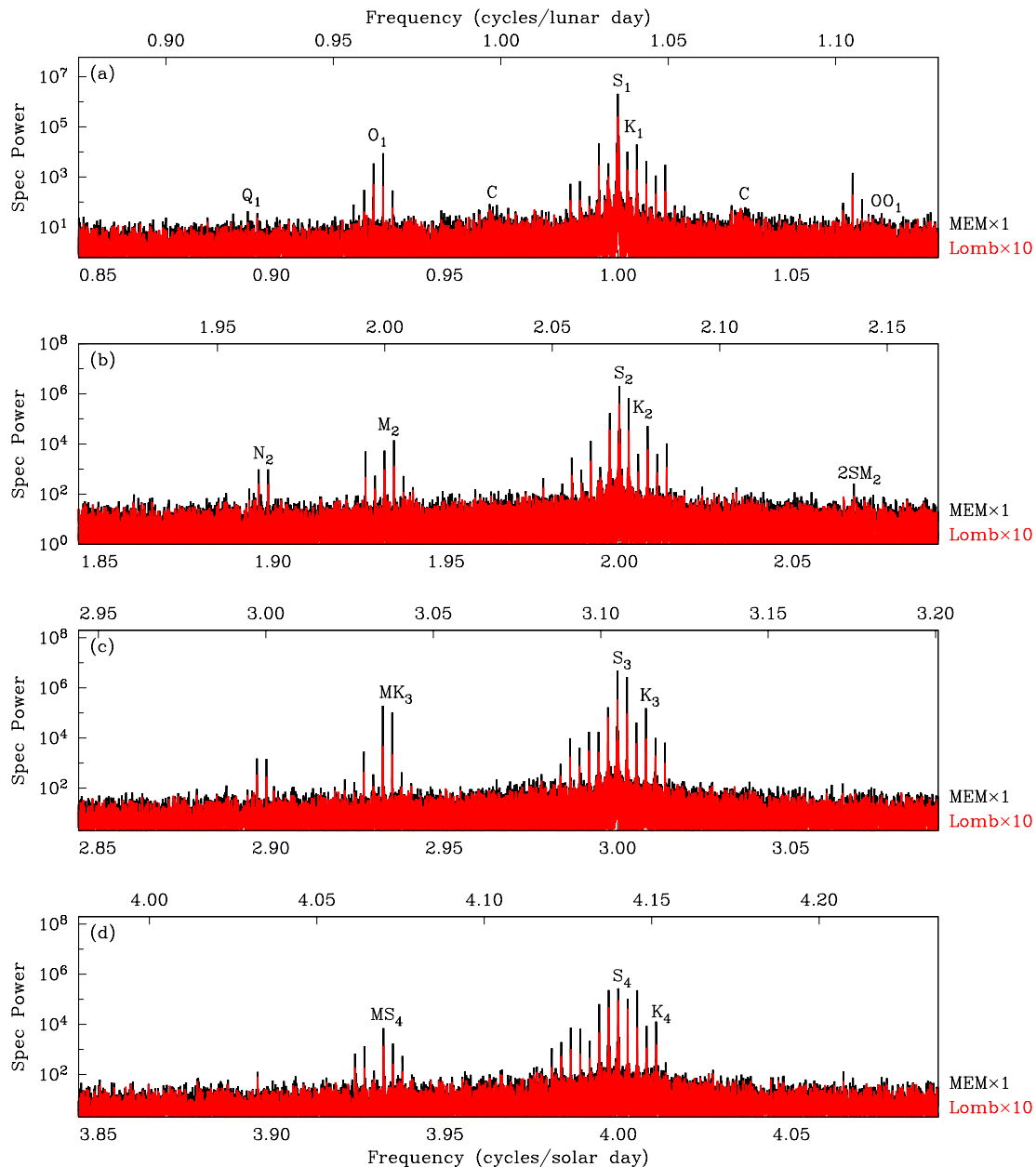


Figure 5. Fine structure of maximum-entropy (MEM, black) and Lomb periodogram (red) power spectra of the pre-whitened first differences (Δ) of HON Z as a function of solar and lunar day frequency near (a) one, (b) half, (c) third, (d) quarter day. Multiplicative factors for clarity are indicated in the margin.

might be related to M_2 by spring-neap splitting of a solar-semidiurnal carrier harmonic, frequencies $2f_{\odot} \pm (2k_m - 2f_a)$. Several gravitational diurnal constituents that are prominent in oceanic tide gauge data, Q_1 , J_1 , OO_1 (Table 2), are barely detectable in the HON data. In Fig. 5(a), we label faint groups of spectral lines that arise from the 13.6-d Carrington overtone of solar rotation and its amplitude modulation of S_1 .

9 HYPERFINE STRUCTURE

Delving, now, into even more detail, in Fig. 6 we note the hyperfine structure surrounding the solar-diurnal, semi-diurnal, etc. constituents $S_{k_{\odot}}$. In each case, after applying multiplicative factors, the maximum-entropy spectrum is neatly draped over the Lomb periodogram spectrum. The diurnal lines are accompanied by sideband

spectral lines, labelled R, representing ~ 11 -yr amplitude modulation (e.g. Chapman & Bartels 1962, Chapter 7.3); similar sidebands are seen for some of the annual constituents, frequencies $k_{\odot}f_{\odot} + k_a f_a \pm f_R$. These modulations are the result of solar-cycle variation in ionizing radiation, which causes variation in ionospheric conductivity and variation in the efficiency of the ionospheric dynamo. Chapman *et al.* (1971) and Malin *et al.* (1975) have reported a similar solar-cycle modulation for the lunar semi-diurnal tide, M_2 , but our spectra do not clearly show this, Fig. 7, and, indeed, other studies have not identified such modulations (De Meyer 1980).

We arrive, finally, at the identification of magnetic tidal constituents that are gravitationally driven by the precession of the lunar perigee, with $T_p = 8.85$ yr, and precession of the lunar nodes, with $T_n = 18.61$ yr. In Fig. 8(a), the presence of the N_2 constituent, frequency $2f_{\zeta} - f_m + f_p$, is clearly seen above background noise,

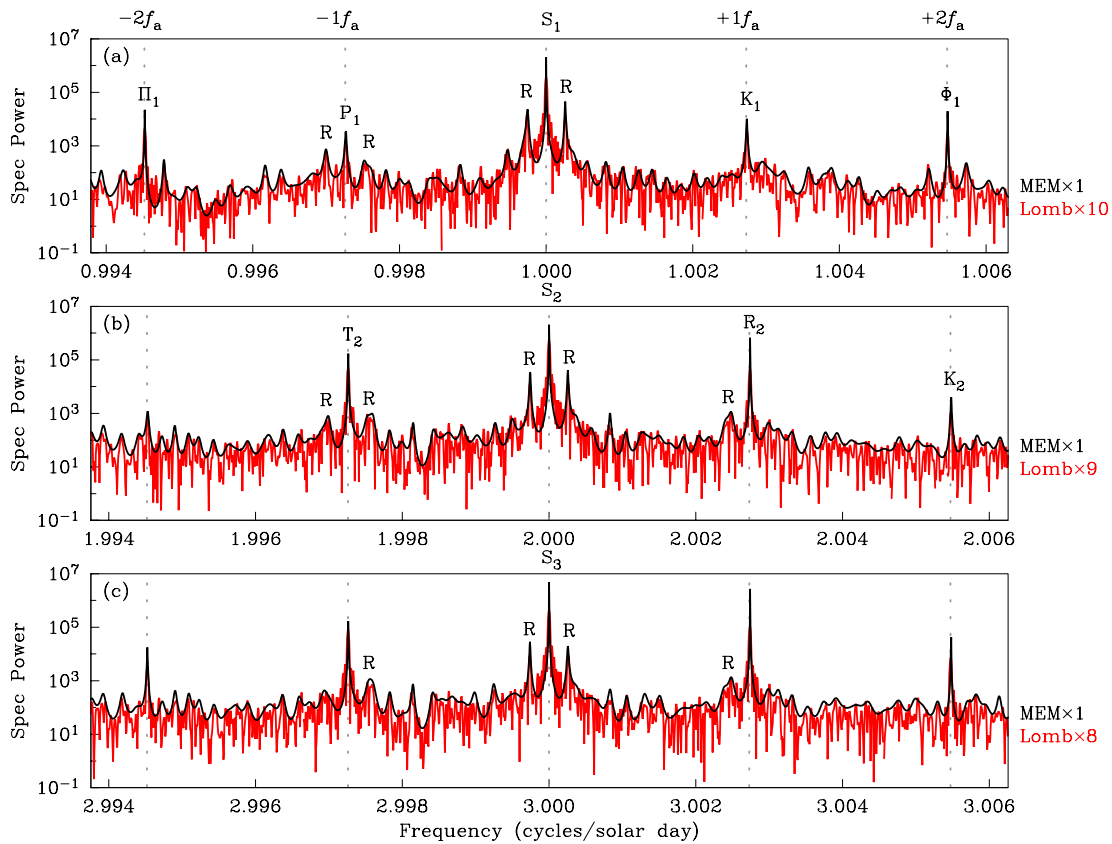


Figure 6. Hyperfine structure of maximum-entropy (MEM, black) and Lomb (red) spectra of HON Z near (a) one, (b) half a solar day, (c) third of a solar day.

as is one of its annual modulation constituents, denoted with a ‘p’. In Fig. 8(b) related lunar perigee tides are also clearly seen near terdiurnal periods. These results lend certainty to previous reported identifications of the N_2 magnetic tide that were made using the old Chapman–Miller method (Leaton *et al.* 1962; Arora & Rao 1975; Palumbo 1981); our spectra are certainly of much higher resolution than those for earlier projects (Currie 1975, fig. 3). Returning to Fig. 7(a), the clearest identification we have been able to make of nodal modulation is a line that is a neighbour of the declinational constituent O_1 ; labelled with an ‘n’, it corresponds to frequency $f_\zeta - f_m - f_n$. We might have expected to find a nodal constituent here, since according to equilibrium gravitational theory, of all the lunar-diurnal tides, nodal modulation of O_1 has the sixth largest potential amplitude (e.g. Cartwright & Tayler 1971, table 4b, Group 1). But the relatively long period of nodal precession makes it challenging to distinguish it from O_1 with only a century of historical data. As far as we know, the presence of this tide, or, indeed, any nodal constituent, in magnetic observatory data have not previously been so clearly demonstrated.

10 SIGNIFICANCE, ROBUSTNESS

Since a periodogram spectrum corresponds to a moving-average model of noise, we can examine the statistical significance of a given periodogram spectral line by comparing its power with that which would be realized from a random process. For Gaussian white noise, the corresponding spectrum would have power distributed according to a χ^2 distribution with 2 degrees of freedom (Emery & Thomson 2001, p. 424). From this, we can estimate the ‘ p -value’

probability that a power greater than that observed for the given spectral line would be realized. Of all the spectral lines discussed here, the most difficult to identify is the ‘n’ nodal modulation $f_\zeta - f_m - f_n$, Fig. 7(a). Compared to the amplitude of the noise spectrum near this spectral line, we estimate that $p < 0.0001$, which is very small, and so it would be a very unlikely realization of random data. This line might, therefore, be reasonably deemed ‘significant’. On the other hand, and as we already noted in Section 6, individual spectral lines identified with a maximum-entropy algorithm do not have physically meaningful amplitude. Indeed, since the principle of maximum entropy is based on the deterministic concepts of autoregression, it is not meaningful to assess particular spectral lines identified in a maximum-entropy spectrum in terms of ‘statistical significance’.

As an additional check of the validity of our identification of spectral lines, we divide the HON data into two subset durations of approximately equal duration, 1915–1959 and 1961–2011, and then construct spectra for each. The latter duration corresponds to uninterrupted operation at a single observatory site (see Section 2). In Fig. 9(a), we show the overall broad perspective from 10 000.0 to 0.1 d. The two subset durations have spectra that are generally similar to those we plot in Fig. 4. We can also see that the spectral line seen in Z at about 0.6250 cycles/solar day (1.6 d and marked with a ‘?’) in the HON data for 1961–2011 is not seen for 1915–1959. Since the existence of this spectral line might just be an insignificant fluke, we cannot reasonably conclude that it corresponds to a previously unidentified tidal constituent. On the other hand, in comparing Fig. 9(b) with 9(c), we can safely conclude that our identification of the ‘n’ tidal constituent for nodal modulation of O_1 is reasonably robust.

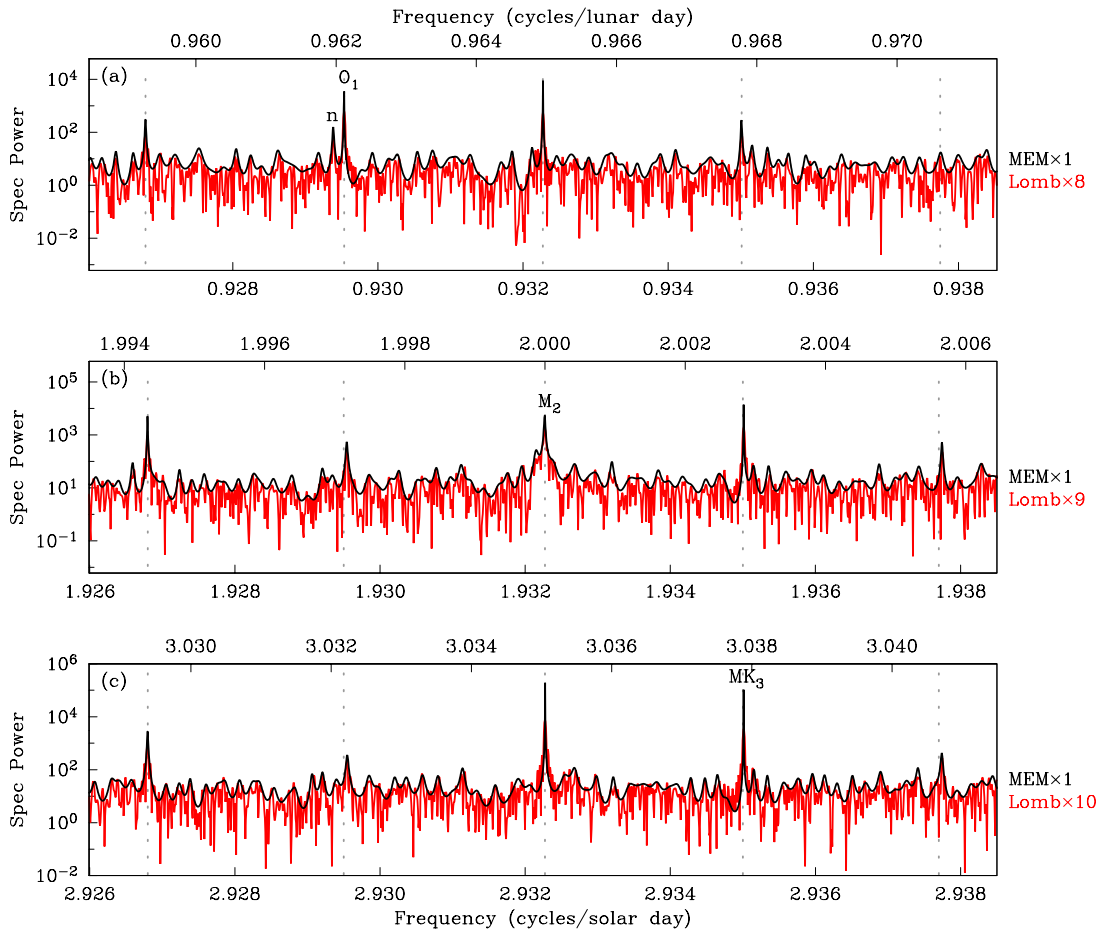


Figure 7. Maximum-entropy (MEM, black) and Lomb (red) spectra of HON Z for lunar semi-diurnal constituents and their solar-diurnal modulations.

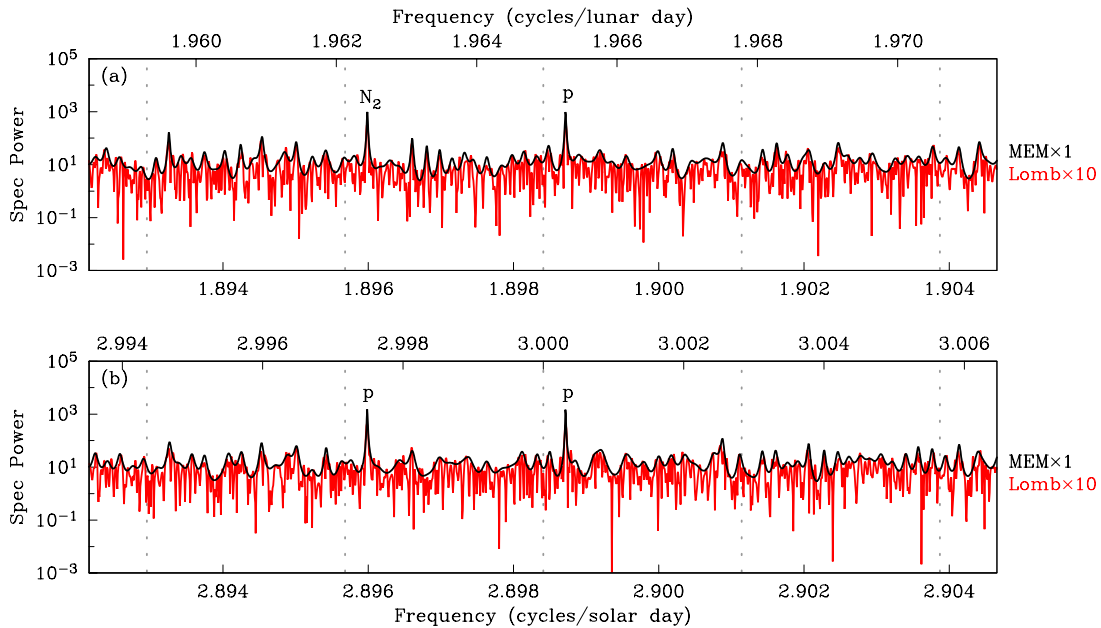


Figure 8. Maximum-entropy (MEM, black) and Lomb (red) spectra of HON Z of lunar eccentricity constituents and their solar-diurnal modulations.

11 RETURN TO THE TIME DOMAIN

Having focussed, in the past few sections of this report, on an examination of magnetic tides in the frequency domain, we now return

to the time domain. Using a least-squares algorithm (Press *et al.* 1992, Chapter 15.4, ‘lfit’), we fit Fourier harmonics corresponding to the constituents listed in Table 2 to each of the HON magnetic vector components: for each constituent frequency f , we obtain

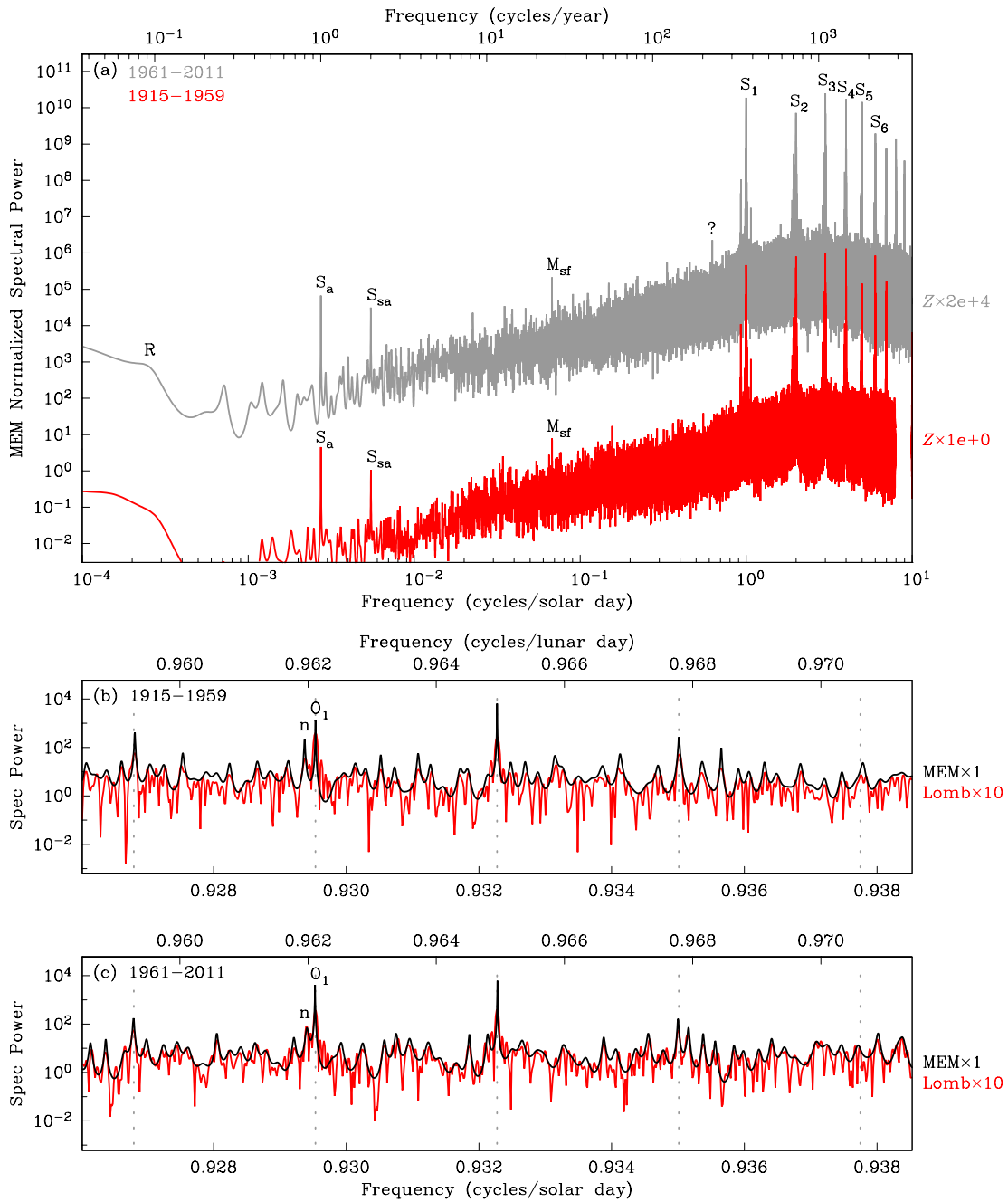


Figure 9. Maximum-entropy (MEM) and Lomb spectra for two subsets of the HON data, 1915–1962 and 1964–2011. Compare with Figs 4 and 7(a).

amplitudes A and phases by minimizing the squared residual difference between each sequence of data and the corresponding Fourier model tidal constituent. We also calculate the percentage of variance reduction ρ for each Fourier constituent for pre-whitened first differences Δ . The tidal constituents listed in Table 2 account for 16 per cent, 63 per cent and 58 per cent of the variance of the first differences of the HON (H , D , Z) data; recall from Section 3 that much of the variation recorded in H is non-tidal magnetic storm activity. For direct inspection, we form synthetic model time-series from a superposition of the discrete-frequency constituent fits listed in Table 2. These synthetic models represent long-term average tidal variation, and we plot them in Figs 1, 2 and 3 (blue, brown, red),

where they reveal annual and solar-cycle modulation of magnetic tides.

In Fig. 10(a), we plot time-series variation of the Table 2 constituent fit for HON Z for 1915–2011. A moving average of this time-series would show almost no solar-cycle variation—note from the discussion of Section 5 that the modulating part of the multiplication of two Fourier harmonics will not, in general, have its own spectral line. We also note that the T_R constituents listed in Table 2 explain only a tiny part of the variance in the data. On the other hand, in Fig. 10(b) we plot the corresponding daily range of Z tidal variation. This shows prominent solar-cycle variation; if we had chosen to construct a power spectra of daily ranges, they

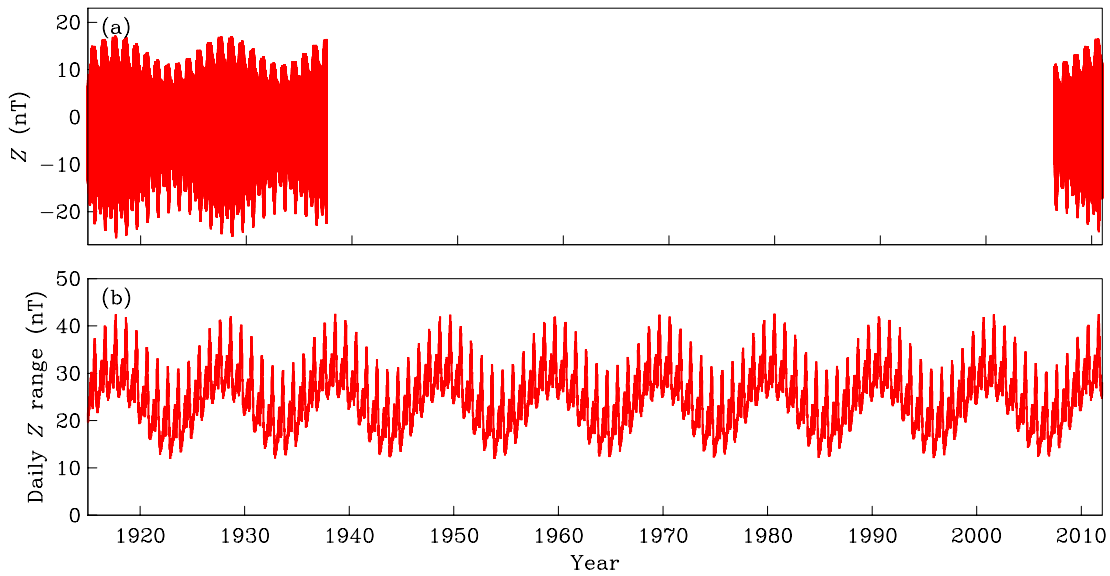


Figure 10. For the constituents listed in Table 2, (a) time-series for HON Z and (b) the corresponding daily range, 1915–2011.

would show prominent lines at ~ 11 -yr. For related reasons, magnetic activity indices, which typically measure the range in non-tidal activity over a chosen duration of time, also show a prominent line at ~ 11 -yr.

Next, we illustrate the amplitude and phase relationship between different magnetic tidal constitutions (e.g. Chapman & Bartels 1962, Chapter 7.2): for selected constituents, we plot the curve traced out by the magnetic vector over the course of a given day. In Fig. 11(a), we plot horizontal-component (X , Y) traces for a typical day for each month of the year. Clearly seen is annual modulation of the synodic solar-diurnal constituents, corresponding to frequencies $k_{\odot}f_{\odot} + k_a f_a$ and the spectral combs near the tides $S_{k_{\odot}}$ in Fig. 5. We note that both the size and shape of the diurnal traces change considerably over the course of a year (e.g. Chapman & Bartels 1962, Chapter 7, fig. 7). In contrast, in Fig. 11(b) we plot horizontal traces corresponding to synodic solar-diurnal constituents $S_{k_{\odot}}$ and their solar-cycle modulations $k_{\odot}f_{\odot} \pm f_R$, minimum to maximum and back to minimum. Here, the size of the diurnal trace changes over the course of a solar cycle, but the shape is mostly constant (e.g. Chapman & Bartels 1962, Chapter 7, fig. 6).

The different types of evolution seen in Figs 11(a) and (b) are related to different combinations of amplitude and phase modulation, both of which are important in the annual modulation, but amplitude is the most important factor for solar-cycle modulation. To emphasize this point, we plot the separate modes for annual modulation of diurnal S_1 constituents $f_{\odot} + k_a f_a$ in Fig. 12(a), semi-diurnal S_2 constituents $2f_{\odot} + k_a f_a$ in Fig. 12(b), etc. Clearly seen is the effect of phase modulation, with the ellipticity of each diurnal mode drifting over the course of a year. In Fig. 11(c), we plot horizontal traces corresponding to sidereal-diurnal constituents $K_{k_{\zeta}}$, frequencies $k_{\zeta}f_{\zeta} + k_{\zeta}f_m$ and their sidereal-monthly modulations due to lunar declination: O_1 , M_2 , MK_3 , MK_4 , frequencies $k_{\zeta}f_{\zeta} + (k_{\zeta} - 2)f_m$, maximum declination to minimum; amplitude and phase modulation are obvious. In Fig. 11(d), we plot traces for the sidereal-diurnal constituents $K_{k_{\zeta}}$ and their modulations due to the precession of the lunar perigee: N_1 and ‘p’ relatives listed in Table 2; small amounts of amplitude and phase modulation are seen.

12 SOME TIDES NOT FOUND

We do not find several tidal signals that have been previously identified by other investigators. Consider, first, the ‘low-frequency’ end of Fig. 4. Rao & Rangarajan (1978) reported finding a ~ 427 -d spectral line corresponding to the pole tide of the Chandler wobble in magnetic observatory data; we do not find a corresponding line in either the maximum-entropy spectrum or Lomb periodogram from HON data. We also do not find a ~ 17 -yr spectral line, possibly related to the Sun, that Juckett (1998) reported finding in magnetic observatory data. We do not find a ~ 22 -yr line corresponding to the Hale solar dynamo cycle (two sunspot cycles) that Currie (1976) reported finding in a global magnetic activity index (non-tidal). We note that Courtillot *et al.* (1977) had difficulty finding a ~ 22 -yr line for the same index, and Prestes *et al.* (2006) could not find it at all. Next, turning to the ‘high-frequency’ diurnal end of the spectra, Olsen (1994) reported finding a ~ 27 -month amplitude modulation of solar-diurnal magnetic tide, and he reported its correlation with the thermosphere quasi-biennial oscillation. Subsequently, Jarvis (1996) reported finding a similar modulation of the solar semi-diurnal magnetic tide. In our depiction of the HON spectra, such modulations should show up in Fig. 6 as lines with frequencies like $k_{\odot}f_{\odot} \pm \frac{12}{27}f_a$, but we do not find such lines. We also do not find mysterious 2-, 3- and 5-d spectral lines that Yamada (2002) found in magnetic observatory data.

13 CONTEXT AND PERSPECTIVE

Many standard measures of geomagnetic disturbance are defined relative to an estimate of solar-quiet daily variation, Sq, that is typically estimated from just 24 hr of data (e.g. Bartels *et al.* 1939; Mayaud 1980). This practice that can be traced back to the era when observatories collected day-long photographic-paper magnetograms. These days, we know that a single day of data is far too short to properly estimate magnetic tidal constituents, and we also know that standard magnetic disturbance indices contain aliased tidal signals that are not part of what most researchers would classify as disturbance (e.g. Clauer *et al.* 1980; Love & Gannon 2009). This, in turn, has sometimes motivated the description of solar-quiet

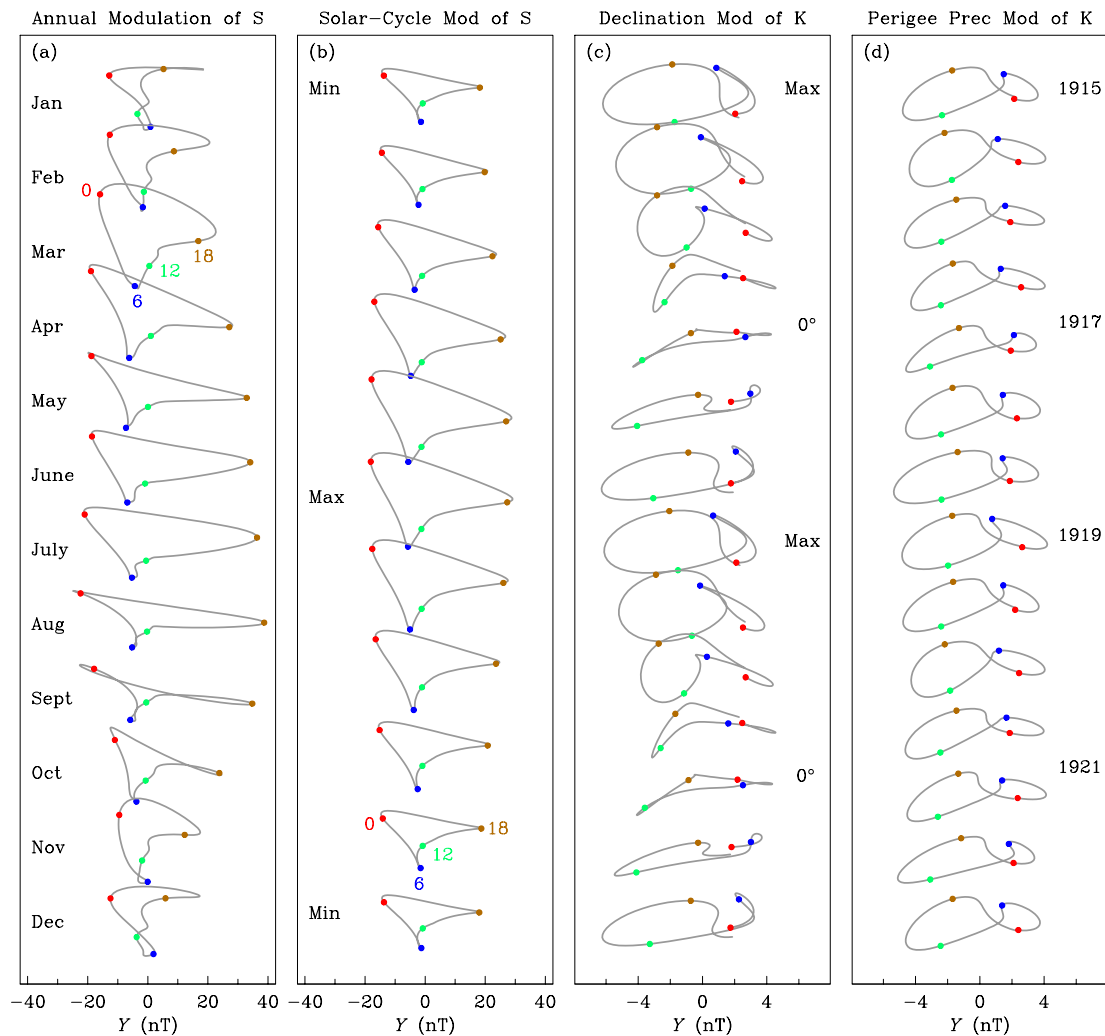


Figure 11. Traces of horizontal-component (X , Y) synodic solar-diurnal constituents and their (a) annual and (b) solar-cycle modulation; sidereal-diurnal variation and their (c) sidereal-monthly and (d) lunar precessional modulations. For (a) and (b), universal-time synodic hours are denoted by red (0), blue (6), green (12), brown (18); for (c) and (d) these markings are relative sidereal hours.

magnetic variation in terms of aperiodic basis functions (e.g. Maslova *et al.* 2009; Mandrikova *et al.* 2013). In light of the preceding analysis, however, we would prefer to define magnetic disturbance relative to a tidal baseline composed of time-invariant periodic Fourier harmonics. Such a definition of disturbance was advocated long ago by Sugiura (1964), who defined the Dst storm-time index relative to a periodic tidal baseline that is composed of solar-diurnal and annual constituents (Sugiura & Kamei 1991).

We conclude with some remarks on time-variant (non-tidal) geomagnetic variation. Its presence in observatory time-series can include non-harmonic time-varying amplitude modulation, $\alpha(t) \cos[\omega t + \phi]$, or non-harmonic time-varying phase modulation, $\alpha \cos[\omega t + \phi(t)]$. Either way, time-variant signals in historical magnetic observatory data can be usefully measured relative to a time-invariant tidal model. Long-term, historical change in the amplitude of magnetic tidal variation has been used, for example, to infer corresponding change in solar irradiance (e.g. Macmillan & Droujinina 2007) and to test the accuracy of historical visual counts of sunspot number (e.g. Svalgaard 2007). Quasi-persistent harmonic oscillations have been identified in magnetic observatory data (Forbes & Leveroni 1996; Liu 1996), and transient

enhancements of lunar magnetic tides (e.g. Bartels & Johnston 1940; Onwumechili 1964) might be correlated with sudden warmings of the stratosphere (e.g. Schoeberl 1978; Fejer *et al.* 2010; Yamazaki *et al.* 2012). The list of time-variant magnetic tidal effects is probably longer than we know, but we are certain that time-invariant periodic magnetic tides will remain a subject of modern scientific importance.

ACKNOWLEDGEMENTS

We thank A. Chulliat, C. A. Finn, J. L. Gannon, D. E. McNamara, M. Moschetti, and an anonymous person for reviewing a draft manuscript. We thank W. F. Denig, B. A. Emery, J. S. Gee, E. A. Kihn, A. Khokhlov, A. Kuvshinov, W. S. Leith, C. Manoj, S. Maus, K. Mursula, J. McCarthy, W. K. Peterson, A. D. Richmond, H. J. Singer, L. Svalgaard, B. T. Tsurutani, and R. H. Tyler for useful conversations. This work was supported by the USGS Geomagnetism Program. Part of this work was accomplished while J. J. Love was supported by the Université Paris, Diderot during his visit of the Institut de Physique du Globe de Paris, 2012 October.

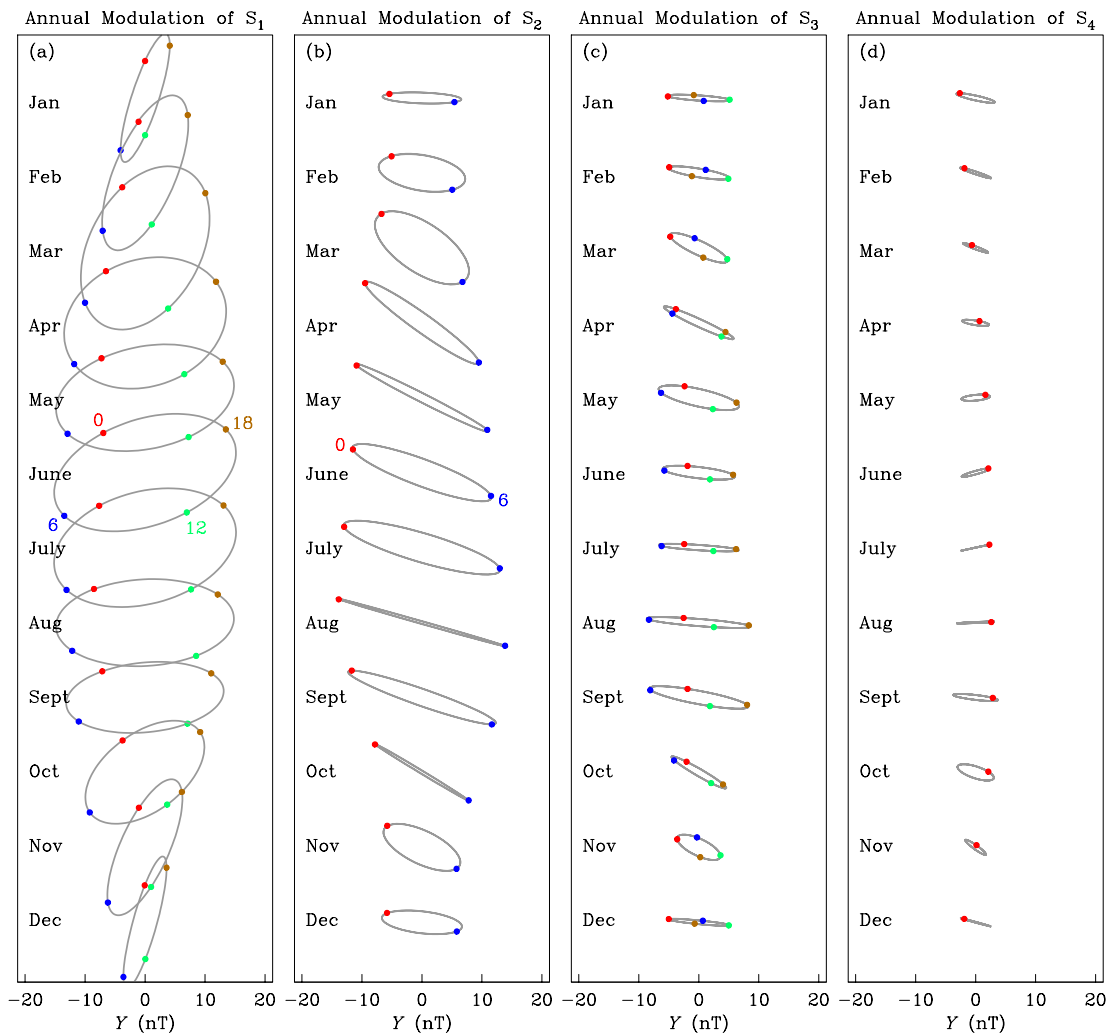


Figure 12. Traces of annual modulation of (a) diurnal, (b) semi-diurnal, (c) terdiurnal and (d) quarter-diurnal horizontal-component synodic constituents. Note that the scale here is half the range of that in Fig. 11(a).

REFERENCES

Arora, B.R. & Rao, D.R.K., 1975. Modulation of geomagnetic lunar daily variation in *H* at Alibag with lunar distance, *Geophys. J. R. astr. Soc.*, **43**, 627–633.

Bartels, J. & Johnston, H.F., 1940. Geomagnetic tides in horizontal intensity at Huancayo, *Terr. Magn. Atmos. Electr.*, **45**, 269–308.

Bartels, J., Heck, N.H. & Johnston, H.F., 1939. The three-hour range index measuring geomagnetic activity, *Terr. Magn. Atmos. Electr.*, **44**, 411–454.

Blackman, R.B. & Tukey, J.W., 1958. *The Measurement of Power Spectra: From the Point of View of Communications Engineering*, Am. Telephone and Telegraph Co. Reprinted by Dover Publications (1959).

Broun, J.A., 1874. *Observations of Magnetic Declination Made at Trevandrum and Agustia Malley in the Observatories of His Highness the Maharajah of Travancore, G.C.S.I. in the Years 1852 to 1869*, Vol. 1, Neill and Company.

Bullard, E.C. & Gellman, H., 1954. Homogeneous dynamos and terrestrial magnetism, *Phil. Trans. R. Soc. Lond., A*, **247**, 213–278.

Campbell, W.H., 1972. A search for an ionospheric dynamo current effect of the galactic X-ray ionization, *Planet. Space Sci.*, **20**, 61–72.

Campbell, W.H., 1982. Annual and semiannual changes of the quiet daily variations (*S_q*) in the geomagnetic field at North American locations, *J. geophys. Res.*, **87**, 785–796.

Canton, J., 1759–1760. An attempt to account for the regular diurnal variation of the horizontal magnetic needle; and also for its irregular variation at the time of an Aurora Borealis, *Phil. Trans. R. Soc. Lond.*, **51**, 398–445.

Cartwright, D.E., 1999. *Tides: A Scientific History*, Cambridge University Press.

Cartwright, D.E. & Tayler, R.J., 1971. New computations of the tide-generating potential, *Geophys. J. R. astr. Soc.*, **23**, 45–74.

CGS, 1909. *Results of Observations Made at the Coast and Geodetic Survey Magnetic Observatory near Honolulu, Hawaii, 1902-1904*, Coast and Geodetic Survey.

CGS, 1918. *Results of Observations Made at the United States Coast and Geodetic Survey Magnetic Observatory near Honolulu, Hawaii, 1915 and 1916*, Coast and Geodetic Survey.

CGS, 1963. *Magnetograms and Hourly Values, Honolulu, Hawaii, 1960*, Coast and Geodetic Survey.

Chapman, S., 1914. On the diurnal variations of the Earth’s magnetism produced by the Moon and the Sun, *Phil. Trans. R. Soc. Lond., A*, **213**, 279–331.

Chapman, S. & Bartels, J., 1962. *Geomagnetism*, Oxford University Press.

Chapman, S. & Raja Rao, K.S., 1965. The *H* and *Z* variations along and near the equatorial electrojet in India, Africa and the Pacific, *J. Atmos. Terr. Phys.*, **27**, 559–581.

Chapman, S., Gupta, J.C. & Malin, S.R.C., 1971. The sunspot cycle influence on the solar and lunar daily geomagnetic variations, *Proc. R. Soc. Lond., A*, **324**, 1–15.

Clauer, C.R., McPherron, R.L. & Kivelson, M.G., 1980. Uncertainty in ring current parameters due to the quiet magnetic field variability at mid-latitudes, *J. geophys. Res.*, **85**, 633–643.

- Courillot, V., Le Mouél, J.L. & Mayaud, P.N., 1977. Maximum entropy spectral analysis of the geomagnetic activity index *aa* over a 107-year interval, *J. geophys. Res.*, **82**, 2641–2649.
- Currie, R.G., 1975. Lunar terms in the geomagnetic spectrum at Hermanus, *J. Atmos. Terr. Phys.*, **37**, 439–446.
- Currie, R.G., 1976. Long period magnetic activity—2 to 100 years, *Astrophys. Space Sci.*, **39**, 251–254.
- Darwin, G.H., 1889. Second series of results of the harmonic analysis of tidal observations, *Proc. R. Soc. Lond.*, **45**, 556–611.
- De Meyer, F., 1980. Solar and lunar daily geomagnetic variations at Dourbes, *J. Atmos. Terr. Phys.*, **42**, 753–763.
- Doodson, A.T., 1928. The analysis of tidal observations, *Phil. Trans. R. Soc. Lond., A*, **227**, 223–279.
- Echer, E., Tsurutani, B.T. & Gonzalez, W.D., 2012. Extremely low geomagnetic activity during the recent deep solar cycle minimum, in *Comparative Magnetic Minima: Characterizing Quiet Times in the Sun and Stars, Proceedings of the IAU Symposium*, Vol. 286, eds Mandrini, C.H. & Webb, D.F., Cambridge University Press, pp. 200–209.
- Emery, W.J. & Thomson, R.E., 2001. *Data Analysis Methods in Physical Oceanography*, Elsevier.
- Fejer, B.G., Olson, M.E., Chau, J.L., Stolle, C., Lühr, H., Goncharenko, L.P., Yumoto, K. & Nagatsuma, T., 2010. Lunar-dependent equatorial ionospheric electrodynamic effects during sudden stratospheric warmings, *J. geophys. Res.*, **115**, A00G03, doi:10.1029/2010JA015273.
- Fejer, J.A., 1964. Atmospheric tides and associated magnetic effects, *Rev. Geophys.*, **2**, 275–309.
- Forbes, J.M. & Leveroni, S., 1996. Quasi 16-day oscillation in the ionosphere, *Geophys. Res. Lett.*, **19**, 981–984.
- Ghil, M. & Taricco, C., 1997. Advanced spectral methods, in *Past and Present Variability of the Solar-Terrestrial System: Measurement, Data Analysis and Theoretical Models*, pp. 137–159, eds Castagnoli, G.C. & Provenzale, A., Soc. Ital. di Fis.
- Graham, G., 1724. An account of observations made of the variation of the horizontal needle at London, in the latter part of the year 1722, and beginning of 1723, *Phil. Trans. R. Soc. Lond.*, **33**, 96–107.
- Hansteen, C., 1819. *Untersuchungen über den Magnetismus der Erde*, Vol. 1, Gedruckt bey J. Lehmann und C. Gröndahl, Christiania.
- Heelis, R.A., 2004. Electrodynamics in the low and middle latitude ionosphere: a tutorial, *J. Atmos. Solar-Terr. Phys.*, **66**, 825–838.
- Hendershott, M. & Munk, W., 1970. Tides, *Ann. Rev. Fluid Mech.*, **2**, 205–224.
- Jankowski, J. & Sucksdorff, C., 1996. *Guide for Magnetic Measurements and Observatory Practice*, IAGA.
- Jarvis, M.J., 1996. Quasi-biennial oscillation effects in the semidiurnal tide of the Antarctic lower thermosphere, *Geophys. Res. Lett.*, **23**, 2661–2664.
- Jay, D.A. & Kukulka, T., 2003. Revising the paradigm of tidal analysis—the uses of non-stationary data, *Ocean Dyn.*, **53**, 110–125.
- Juckett, D.A., 1998. Evidence for a 17-year cycle in the IMF directions at 1 AU, in solar coronal hole variations, and in planetary magnetospheric modulations, *Solar Phys.*, **183**, 201–224.
- Kanasewich, E.R., 1981. *Time Sequence Analysis in Geophysics*, University Alberta Press.
- Kelley, M.C., 1989. *The Earth's Ionosphere: Plasma Physics and Electrodynamics*, Academic Press.
- Korn, G.A. & Korn, T.M., 2000. *Mathematical Handbook for Scientists and Engineers*, Dover.
- Kreil, K., 1852. Einfluß des Mondes auf die magnetische Deklination, *Denkschr. Akad. Wiss. Wien Math.-Naturw. Kl.*, **3**, 1–47.
- Kuvshinov, A.V., 2012. Deep electromagnetic studies from land, sea, and space: progress status in the past 10 years, *Surv. Geophys.*, **33**, 169–209.
- Lakhan, V.C., 2005. Time series modeling, in *Encyclopedia of Coastal Science*, pp. 996–1000, ed. Schwartz, M., Springer-Verlag.
- Larsen, J.C., 1968. Electric and magnetic fields induced by deep sea tides, *Geophys. J. R. astr. Soc.*, **16**, 47–70.
- Leaton, B.R., Malin, S.R. & Finch, H.F., 1962. The solar and luni-solar daily variation of the geomagnetic field at Greenwich and Abinger, 1916–1957, *Royal Obs. Bull.*, **63**, 273–318.
- Lindzen, R.S. & Chapman, S., 1969. Atmospheric tides, *Space Sci. Rev.*, **10**, 3–188.
- Liu, J.Y., 1996. A study of quasi-16-day ionospheric oscillation, *Radiophys. Quantum Electron.*, **39**, 155–165.
- Love, J.J. & Finn, C.A., 2011. The USGS geomagnetism program and its role in space weather monitoring, *Space Weather*, **9**, S07001, doi:10.1029/2011SW000684.
- Love, J.J. & Gannon, J.L., 2009. Revised *Dst* and the epicycles of magnetic disturbance: 1958–2007, *Ann. Geophys.*, **27**, 3101–3131.
- Love, J.J., Tsai, V.C. & Gannon, J.L., 2010. Averaging and sampling for magnetic-observatory hourly data, *Ann. Geophys.*, **28**, 2079–2096.
- Macmillan, S. & Droujinina, A., 2007. Long-term trends in geomagnetic daily activity, *Earth Planets Space*, **59**, 391–395.
- Malin, S.R.C., 1970. Separation of lunar daily geomagnetic variations into parts of ionospheric and oceanic origin, *Geophys. J. R. astr. Soc.*, **21**, 447–455.
- Malin, S.R.C., 1973. Geomagnetic variations with the period of a sidereal day, *Planet. Space Sci.*, **21**, 145–146.
- Malin, S.R.C., Cecere, A. & Palumbo, A., 1975. The sunspot cycle influence on lunar and solar daily geomagnetic variations, *Geophys. J. R. astr. Soc.*, **41**, 115–126.
- Mandrikova, O., Solovjev, I., Geppener, V., Al-Kasabeh, R.T. & Klioskiy, D., 2013. Analysis of the Earth's magnetic field variations on the basis of a wavelet-based approach, *Dig. Signal Process.*, **23**, 329–339.
- Maslova, I., Kokoszka, P., Soja, J. & Zhu, L., 2009. Removal of non-constant daily variation by means of wavelet and functional data analysis, *J. geophys. Res.*, **114**, A03202, doi:10.1029/2008JA013685.
- Matsushita, S., 1967. Solar quiet and lunar daily variation fields, in *Physics of Geomagnetic Phenomena*, Vol. 1, pp. 302–424, eds Matsushita, S. & Campbell, W.H., Academic Press.
- Maus, S. & Kuvshinov, A., 2004. Ocean tidal signals in observatory and satellite magnetic measurements, *Geophys. Res. Lett.*, **31**, L15313, doi:10.1029/2004GL020090.
- Mayaud, P.N., 1980. *Derivation, Meaning, and Use of Geomagnetic Indices*, Geophysical Monograph 22, American Geophysical Union.
- Moos, N.A.F., 1910. *Colaba Magnetic Data, 1846 to 1905. Part II: The Phenomenon and its Discussion*, Government Central Press.
- Nowożyński, K., 2006. On regularities in long-term solar quiet geomagnetic variations, *Earth planet. Sci. Lett.*, **241**, 648–654.
- Olsen, N., 1994. A 27-month periodicity in the low latitude geomagnetic field and its connection to the stratospheric QBO, *Geophys. Res. Lett.*, **21**, 1125–1128.
- Olsen, N., 1997. Geomagnetic tides and related phenomena, in *Tidal Phenomena*, pp. 261–274, eds Wilhelm, H., Zürn, W. & Wenzel, H.G., Springer-Verlag.
- Onwumehili, C.A., 1964. On the existence of days with extraordinary geomagnetic lunar tide, *J. Atmos. Terr. Phys.*, **26**, 720–748.
- Palumbo, A., 1981. Lunar and solar daily variations of the geomagnetic field at Italian stations, *J. Atmos. Terr. Phys.*, **43**, 633–642.
- Parkinson, W.D., 1983. *Introduction to Geomagnetism*, Scottish Academic Press.
- Press, W.H., Teukolsky, S.A., Vetterling, W.T. & Flannery, B.P., 1992. *Numerical Recipes*, Cambridge University Press.
- Prestes, A., Rigozo, N.R., Echer, E. & Vieira, L.E.A., 2006. Spectral analysis of sunspot number and geomagnetic indices (1868–2001), *J. Atmos. Solar-Terr. Phys.*, **68**, 182–190.
- Pugh, D.T., 1987. *Tides, Surges, and Mean Sea-Level*, John Wiley & Sons.
- Rao, D.R.K. & Rangarajan, G.K., 1978. The pole-tide signal in the geomagnetic field at a low-latitude station, *Geophys. J. R. astr. Soc.*, **53**, 617–621.
- Rao, D.R.K. & Sastri, N.S., 1974. The O_1 component of the geomagnetic lunar daily variation in the Indian equatorial region, *J. Geomagn. Geoelectr.*, **26**, 285–293.
- Rastogi, R.G., 1993. Geomagnetic field variations at low latitudes and ionospheric electric fields, *J. Atmos. Solar-Terr. Phys.*, **55**, 1375–1381.
- Richmond, A.D., 1995. Ionospheric electrodynamics, in *Handbook of Atmospheric Electrodynamics*, Vol. 2, pp. 249–290, ed. Volland, H., CRC Press.

- Russell, C.T., Luhmann, J.G. & Jian, L.K., 2010. How unprecedented a solar minimum?, *Rev. Geophys.*, **48**, RG2004, doi:10.1029/2009RG000316.
- Sabine, E., 1857. On the evidence of the existence of the decennial inequality in the solar-diurnal magnetic variations, and its non-existence in the lunar-diurnal variation, of the declination at Hobarton, *Phil. Trans. R. Soc. Lond.*, **147**, 1–8.
- Sanford, T.B., 1971. Motionally induced electric and magnetic fields in the sea, *J. geophys. Res.*, **76**, 3476–3492.
- Schoeberl, M.R., 1978. Stratospheric warmings: observations and theory, *Rev. Geophys. Space Phys.*, **16**, 521–538.
- Stening, R.J., 1995. What drives the equatorial electrojet?, *J. Atmos. Solar-Terr. Phys.*, **57**, 1117–1128.
- Stewart, B., 1882. Hypothetical views regarding the connexion between the state of the Sun and terrestrial magnetism, *Ency. Brit.*, 9th ed., **16**, 181–184, reprinted in 1890.
- Sugiura, M., 1964. Hourly values of equatorial *Dst* for the IGY, *Ann. Int. Geophys. Year*, **35**, 9–45.
- Sugiura, M. & Kamei, T., 1991. *Equatorial Dst index 1957–1986*, IAGA Bull., 40, ISGI Pub. Office.
- Svalgaard, L., 2007. Calibrating the sunspot number using “the magnetic needle”, *CAWSES Newsletter*, **4**(1), 6–8.
- Tarpley, J.D., 1971. The O₁ component of the geomagnetic lunar daily variation, *J. Geomagn. Geoelectr.*, **23**, 169–179.
- Tyler, R.H., Maus, S. & Lühr, H., 2003. Satellite observations of magnetic fields due to ocean tidal flow, *Science*, **299**, 239–241.
- Vallado, D.A., 2007. *Fundamentals of Astrodynamics and Applications*, Springer-Verlag.
- van Bemmelen, W., 1912. Die lunare variation des Erdmagnetismus, *Meteorol. Z.*, **29**, 218–230.
- Volland, H., 1988. *Atmospheric Tidal and Planetary Waves*, Kluwer Academic Press.
- Winch, D.E., 1970. Geomagnetic lunar tides, O₁ component, *J. Geomagn. Geoelectr.*, **22**, 319–328.
- Winch, D.E., 1981. Spherical harmonic analysis of geomagnetic tides, 1964–1965, *Phil. Trans. R. Soc. Lond., A*, **303**, 1–104.
- Yamada, Y., 2002. 2-day, 3-day, and 5-6-day oscillations of the geomagnetic field detected by principal component analysis, *Earth Planets Space*, **54**, 379–392.
- Yamazaki, Y., Richmond, A.D. & Yumoto, K., 2012. Stratospheric warmings and the geomagnetic lunar tide: 1958–2007, *J. geophys. Res.*, **117**, A04301, doi:10.1029/2012JA017514.